International Journal of Energy and Power Engineering
2024, Vol. 13, No. 5, pp. 73-96
https://doi.org/10.11648/j.ijepe.20241305.11

Research Article

Adaptive Generalized Extended State Observer for a Single Phase PV Grid-connected System Operating Under the Sudanese-Sahelian Climate of Cameroon

Yaouba[1, 2, *], Albert Ayang[1], Ahmat Tom[3], Noël Djongyang[1]

[1]Department of Renewable Energy, National Advance School of Engineering of Maroua, University of Maroua, Maroua, Cameroon

[2]Research Centre for Renewable Energy, Institute of Geological and Mining Research, Yaoundé, Cameroon

[3]Department of Energy Engineering, University Institute of Technology, University of Ngaoundéré, Ngaoundéré, Cameroon

Abstract

Knowing the health of a system allows to guarante its efficiency and sustainability. The state observer is one of several techniques used by authors to estimate system state. This paper focuses on the problem of simultaneous states estimation of DC (Direct Current) and AC (Alternating Current) sides of a single-phase Photovoltaic (PV) grid-connected operating under the Sudanese-Sahelian climate of Cameroon. A generalized extended state observer (GESO) has been designed to simultaneously estimate the three states and the three disturbances of the system. A good estimation of the state and disturbances is achieved by the appropriate choice of the observer gain and the disturbance compensation gain resulting from the correct pole placement. The GESO robustness has been tested by varying the PV voltage and grid voltage. When there are no input fluctuations, the estimation errors of nominal states and disturbances converge to zero. The fluctuation in PV voltage resulting from partial shading has a significant impact on the boost converter current. The boost converter current varies proportionally with the drop in voltage due to partial shading from 55% to 59%. Under the grid voltage fluctuation, the boost converter current remains stable while the DC bus voltage and inverter current are significantly affected. The proposed GESO prove its robustness to perturbations from the PV array and grid side into the Single-Phase PV Grid-connected System. This paper contributes to the study of observers applied to the PV system and points the way to future work on diagnosing faults in PV systems operating in Cameroon's Sudanese-Sahelian climate.

Keywords

Generalized Extended State Observer, Active Disturbance Rejection Control, PV Grid-Connected System, Sudanese-Sahelian Climate, Cameroon

[*]Corresponding author: yaoubadams21@gmail.com (Yaouba)

Received: 24 September 2024; **Accepted:** 16 October 2024; **Published:** 11 November 2024

1. Introduction

1.1. Background

The availability, quality and sustainable management of electrical energy is one of the world's major energy challenges, as the population grows rapidly and fossil fuels become increasingly scarce [1]. In Cameroon, more than 50% of the country's electricity comes from hydroelectric power [2]. Because of climate change in recent years, hydropower is affected by hydrological variability and decreases during periods of low rainfall. To address these issues, the Cameroonian government launched a rural electrification project using solar photovoltaic energy. As renewable energy is an attractive option for electrifying remote areas, this policy is a first step towards solving the problem of energy availability. However, due to the remoteness of the installation sites, the maintenance of solar power plants is an issue which requires special attention, since parameters such as variations in irradiance, temperature, angle of incidence, shading, dust deposits, etc., influence significally the PV system efficiency [3, 4]. To prevent energy loss and equipment damage, a proper and early fault detection is very important [5].

1.2. Related Work

Many significant monitoring and PV diagnosis techniques are developed. Visual inspection and imaging-based methods such as infrared (IR) thermography, ultraviolet (UV) fluorescence, photoluminescence (PL) and electroluminescence (EL) are widely used. However, these techniques consume time and require additional expensive equipment [6]. Apart from fact that additional equipment, such as sensor redundancy, is expensive; the reliability of the sensors has to be constantly monitored to avoid false readings. To deal with these problems, state observer method is used to reconstruct the system's state based on the knowledge of its inputs and outputs [7, 8].

Observers are designed to estimate state or disturbance of a system. There are several types of observers described in the literature, such as adaptive observer, extended state observers, sliding mode observer (SMO), unknown input observer (UIO), learning observer (LO), disturbance observer, perturbation observer, equivalent input disturbance (EID) based estimation, Extended State Observer (ESO) [9-23]. Disturbances Observers-based control are classified into two categories by [24]: linear disturbance and uncertainty estimation (LDUE) techniques, and nonlinear disturbance and uncertainty estimation (NDUE). The Extended State Observer is a fundamental part of Active Disturbance Rejection Control (ADRC), which goal is to eliminate unknown uncertainties and external disturbances. Proposed the first time by Han in 1990, ADRC is a practical alternative to classical proportional-integral-derivative (PID) control [24, 8]. The GESO differs from other observers by minimizing the influence of uncertainties on the output of the studied system, whether the unknown disturbances are accurately estimated or not. On the other hand, the main question is whether UIO and sliding mode observer approaches can accurately reconstruct an unknown disturbance. Perturbation-based feedforward control for systems with mismatched uncertainties has been an unsolved problem for a long time. Therefore, it is important to consider a more restrictive condition for the design of the observer [25]. This should take into account the operating conditions and the specificity of each system studied.

Shah and Singh (2020) proposed a multifunctional adaptive observer for a solar energy conversion [26]. Alshiekh et al. (2020) proposed a control scheme to maintain the system stable and eliminate the effect of the computation delay. Based on measuring the injected current, they performed an estimation of filter capacitor current using the discrete -time observer [27].

Because of voltage and current sensor disadvantages and to minimize the number of sensors required, Mokhlis et al. (2020) designed the high gain observer to rapidly and accurately determine the desired global maximum power point [28].

Wang et al. (2015) studied the mismatched disturbance rejection control problem. By using the disturbance estimation technique based on ESO, the proposed controller not only makes the states of a closed-loop system obtain better tracking performance but also provides better disturbance rejection ability against resistance load variation [29].

When an LCL filter is applied to remove power electronic chopping harmonics, the power quality faces two issues: resonance damping and grid voltage-induced current distortion. Two separate control algorithms requiring an additional current sensor, increasing control complexity and limiting performance, conventionally solve this problem. To deal with that, a current control strategy based on linear ADRC for a grid-connected inverter with an LCL filter to enhance power quality is proposed by Wang et al. (2018) [30]. The proposed strategy can realize active damping and suppression of grid voltage-induced current distortion at the same time in the same control structure with fewer sensors. Moreover, it can give better performance in both dynamic and steady states.

Uncertainties due to variations in component parameters and changes in climatic conditions have a serious impact on the control performance of the inverter. To overcome this problem, Zhu and Fei (2018) proposed to estimate disturbances in real-time by using a sliding mode to control the output voltage of the DC-AC inverter, and a fuzzy logic to approximate the upper bound of the observation error between the actual disturbance and its observed value [31].

Fast-varying sinusoidal disturbances are disturbances in the phase, frequency or magnitude of sinusoidal signals. The conventional extended state observer (ESO) cannot handle these fast perturbations. In response to these issues, Guo et al. (2021) developed the Generalized Integrator-Extended State

Observer and applied it to grid-connected converters in the presence of disturbances. In particular, the case of a three-phase phase-locked loop with noisy regimes is studied. The proposed observer solves the trade-off between the bandwidth of the observer and the noise filtering [32].

Jain et al. (2017) presented a robust fault detecting and identifying scheme based on a linearly switched Luenberger observer for DC-DC power electronic converters. The proposed scheme includes a fault diagnosis filter detecting a fault event and a bank of fault identification filters identifying a faulty converter component. With a suitable gain matrix design, the residual function converges to zero in the absence of faults and is robust in the presence of noise and other non-idealities [33].

Qin (2020) discuss the double current loop control strategy of a single-phase LCL grid- connected inverter based on the Luenberger state observer. This strategy solves the problems of sensor installation and measurement noise [34].

To improve the control of grid-connected inverters under unbalanced grid voltage conditions, Benyamina et al. (2021) proposed an extended state observer - based sensorless control. Positive and negative sequence components are estimated [13].

Generalized Active Disturbance Rejection Control (GADRC) applied to the boost converter was tested by Ayang (2020). The results of this work show that the extended generalized state observer is robust to disturbances, but the control that is used does not follow the fixed references during the disturbed periods [35].

1.3. Key Research Gap

Like other industrial processes, photovoltaic systems are subject to several uncertainties, such as parameter perturbation, external disturbances and non-linear loads [36]. The integration of PV generation into the grid brings different challenges affecting the stability of the grid [37]. Thus, because the reliability and durability of PV installation have an significant impact on the cost investment, it is necessary and imperative to know the status of the system in real-time [38]. Several important approaches have been developed in the literature to meet these requirements, and we have listed a few of them above. However, these approaches are either state estimators or disturbances estimators [39, 24, 31, 40]. Few approaches are both state and disturbances estimators. On the other hand, in most of the works using the observer method in photovoltaic systems, the authors are interested in either the DC side or the AC side [29, 41, 34, 42]. In addition, the ADRC approach, which emphasizes the use of the Extended State Observer (ESO) to timely estimate and eliminate the effect of the total disturbance, including both internal unmodeled dynamics and external disturbances in the system shows more significant results among many significant approaches based on state and disturbance estimation developed in the literature [43]. A major asset of this paper is the application of this approach to photovoltaic systems, considering both the DC and AC sides.

1.4. Motivations and Paper's Main Contributions

In this work, the aim is to propose an Adaptive Observer capable of estimating both the states and the disturbances of a photovoltaic system and eliminating the effect of mismatched uncertainties. The robustness test is based on the work of Yaouba et al. (2022) who demonstrated that in the Sudanese-Sahelian zone of Cameroon, when shading varies from 60% to 95%, PV voltage decreases from 55% to 59% [44]. The main contributions of this paper are illustrated as follows:

1) The application of the Adaptive GESO to photovoltaic systems, considering both the DC and AC sides,
2) Design of the nominal and extended state observer with two controls (one control on DC side and one control on AC side),
3) Simultaneous estimation of system states and unmodeled dynamics,
4) Evaluating of the GESO robustness applied to the single-phase grid-connected PV system operating under the Sudanese-Sahelian climate of Cameroon,
5) Assessing the effects of the external disturbances from the DC and AC sides of the studied system.

This paper is organized as follows: The model of the system is illustrated in Section 2 by the general GESO approach and the studied system topology. In section 3, the proposed observer is constructed. Section 4 presents the simulation results. The conclusion and outlook are given in section 5.

2. Model of Studied System

2.1. The GESO Approach

Let us consider an uncertain system with the order of n described in [25]:

$$\begin{cases} \dot{x}_1 = x_2 \\ \dot{x}_2 = x_3 \\ \quad \vdots \\ \dot{x}_n = f(x_1,...,x_n,w(t),t)+bu \\ y = x_1 \end{cases} \tag{1}$$

The states are $x_1,...,x_n$, the control input is u, the output is y, the external disturbance is $\omega(t)$, b is a system parameter, and $f(x_1,...,x_n,\omega(t),t)$ represents the uncertain function or lumped disturbance.

The system (1) can be linearized by introducing an additional variable:

$$x_{n+1} = f(x_1,...,x_n,w(t),t) \tag{2}$$

The extended state equation resulting from combining (1) with (2) is given by:

$$\begin{cases} \dot{x}_1 &= x_2 \\ \dot{x}_2 &= x_3 \\ &\vdots \\ \dot{x}_n &= x_{n+1} + bu \\ \dot{x}_{n+1} &= h(t) \\ y &= x_1 \end{cases} \tag{3}$$

With $h(t) = \dot{f}(x_1, ..., x_n, w(t), t)$

A general MIMO (Multiple Input, Multiple Output) system includes multiple disturbances is defined as follows [25]:

$$\begin{cases} \dot{x} &= Ax + B_u u + B_d f(x, w(t), t) \\ y_m &= C_m x \\ y_0 &= C_0 x \end{cases} \tag{4}$$

Where $x \in R^n$ is the system's state vector, $u \in R$ is the system input, $\omega \in R$ represents the external disturbance, and $y_m \in R^r$ and $y_o \in R$ are measurable and controlled outputs, respectively. The system matrices are respectively A with dimension $n \times n$, B_u with dimension $n \times 1$, B_d with dimension $n \times 1$, C_m with dimension $r \times n$, and C_o with dimension $1 \times n$.

$f(x, \omega(t), t)$ is the uncertain function in terms of x and, ω representing the lumped disturbance, which is a generalized concept, possibly including external disturbances, unmodeled dynamics, parameter variations, and complex nonlinear dynamics.

As in system (1), the system (4) can be linearized by adding an extended variable:

$$x_{n+1} = d = f(x, w(t), t) \tag{5}$$

Thus, the extended system equation is obtained as:

$$\begin{cases} \dot{\bar{x}} &= \bar{A}\bar{x} + \bar{B}_u u + Eh(t) \\ y_m &= \bar{C}_m \bar{x} \end{cases} \tag{6}$$

With variables $\bar{x} = \begin{bmatrix} x \\ x_{n+1} \end{bmatrix}$; $h(t) = \dfrac{df(x, w(t), t)}{dt}$; and matrices

$$\bar{A} = \begin{bmatrix} A_{n\times n} & (B_d)_{n\times 1} \\ 0_{n\times 1} & 0_{1\times 1} \end{bmatrix}_{(n+1)\times(n+1)}; \quad \bar{B}_u = \begin{bmatrix} (B_u)_{n\times 1} \\ 0_{1\times 1} \end{bmatrix}_{(n+1)\times 1};$$

$$E = \begin{bmatrix} 0_{n\times 1} \\ 1_{1\times 1} \end{bmatrix}_{(n+1)\times 1}; \quad \bar{C}_m = \begin{bmatrix} C_m & 0_{r\times 1} \end{bmatrix}_{r\times(n+1)}$$

From system equation (6), the GESO is derived as follows:

$$\begin{cases} \dot{\hat{\bar{x}}} &= \bar{A}\hat{\bar{x}} + \bar{B}_u u + L(y_m - \hat{y}_m) \\ \hat{y}_m &= \bar{C}_m \hat{\bar{x}} \end{cases} \tag{7}$$

Where $\hat{\bar{x}} = \begin{bmatrix} \hat{x}^T & \hat{x}_{(n+1)} \end{bmatrix}^T$, with $\hat{\bar{x}}$, $\hat{x}$ and $\hat{x}_{(n+1)}$ the state variable estimates of $\bar{x}$, x and $x_{(n+1)}$, respectively. Matrix L with dimension $(n + 1) \times r$ is the observer gain to be designed.

2.2. Studied system Topology

This section presents the model of a single-phase PV system connected to the grid, and the equivalent circuit diagram and the equations of the dynamic system. The equivalent circuit of the system studied is shown in Figure 1. It consists of a PV module, a DC-DC converter, a single-phase inverter, a filter L and the grid part represented by the voltage V_g. In the PV part, G and T are the irradiance and temperature respectively. The type of converter used in this work is a boost converter. I_{pv} is the PV module current; L_b, I_{Lb} and R_{Lb} are respectively the smoothing inductance, the inductance current and the resistance of the boost converter. L_b and R_{Lb} are used to limit the current ripple in the converter. The power switch S_b (MOSFET, IGBT) coupled to the diode D ensures the transfer of energy to the load. The ripple caused by switching at the output of the converter is reduced by the filter capacitor C_{dc}. The DC-DC converter and the single-phase inverter are controlled by PWM (Pulse Width Modulation) modulators that generate pulses with a frequency of $f=1/T$ and a width of μT, where $\mu \in [0,1]$ is the duty cycle of the control pulses. I_{inv}, R_{Linv}, and L_{inv} are respectively the current, the resistance and the inductance of the inverter controlled by the switches S_1, S_2, S_3 and S_4.

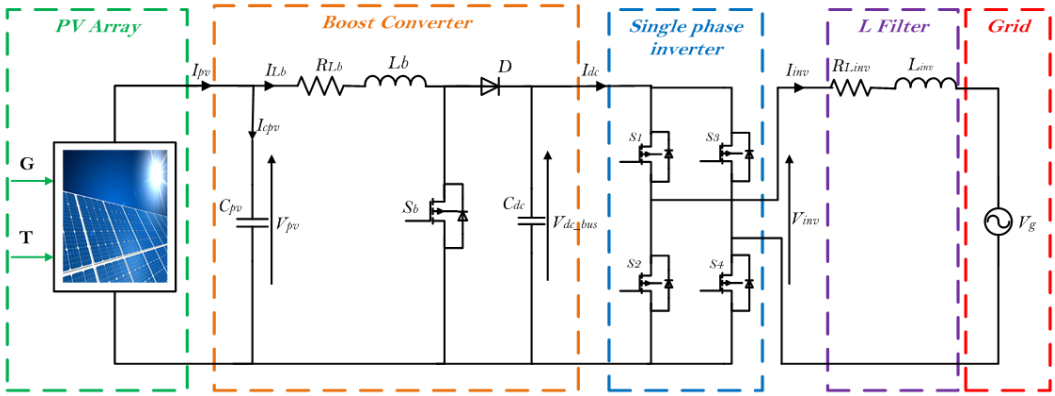

Figure 1. *System equivalent circuit.*

The equivalent circuits shown in Figures 2-5 illustrate respectively the energy accumulation and the energy transfer phases described by four conduction sequences.

2.2.1. Energy Accumulation Phase in the Smoothing Inductor L_b

Conduction sequence 1: S_b closed and D blocked (converter side, μ_1=1); S_1, S_4 closed and S_2, S_3 opened (inverter side, μ_2=1)

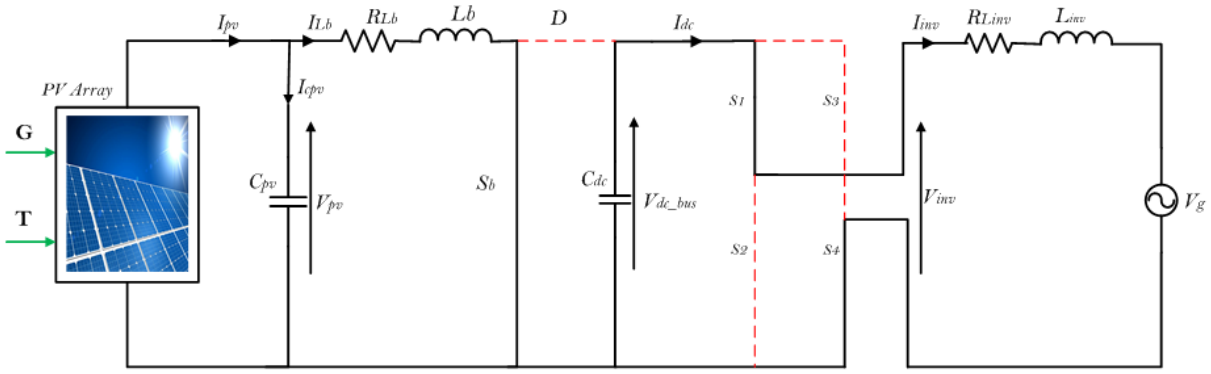

Figure 2. *Energy accumulation phase 1.*

The dynamic model of the system is described by the equations (8)-(11) from this equivalent circuit.

$$\begin{cases} \dfrac{dI_{Lb}}{dt} = -\dfrac{R_{Lb}}{L_b} I_{Lb} + \dfrac{V_{pv}}{L_b} \\ \dfrac{dV_{dc\_bus}}{dt} = -\dfrac{1}{C_{dc}} I_{inv} \\ \dfrac{dI_{inv}}{dt} = \dfrac{1}{L_{inv}} V_{dc\_bus} - \dfrac{R_{Linv}}{L_{inv}} I_{inv} - \dfrac{V_g}{L_{inv}} \end{cases} \tag{8}$$

Conduction sequence 2: Sb closed and D blocked (converter side μ_1=1); S_1, S_4 opened and S_2, S_3 closed (inverter side μ_2=0)

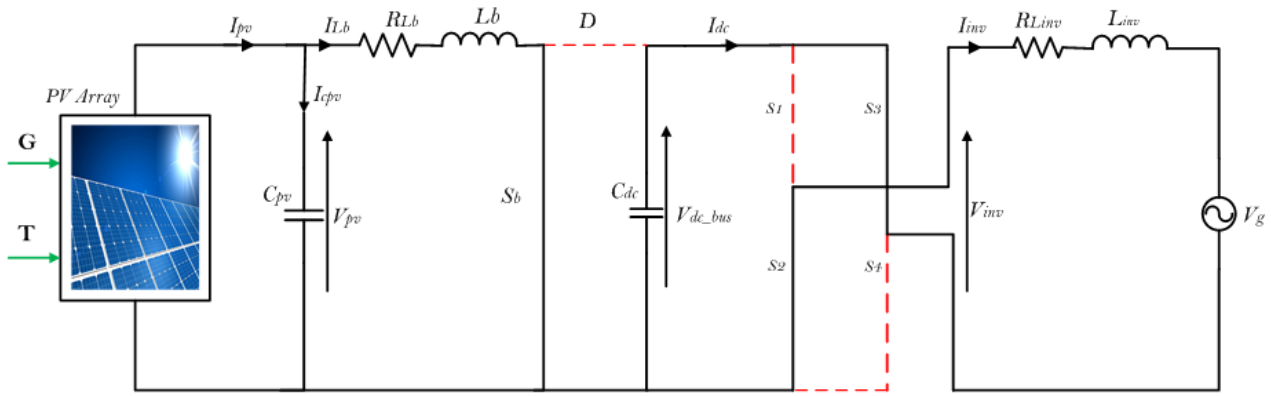

Figure 3. *Energy accumulation phase 2.*

2.2.2. Energy Transfer Phase

Conduction sequence 3: Sb open and D open (converter side μ_1=0); S_1, S_4 closed and S_2, S_3 opened (inverter side μ_2=1)

$$\begin{cases} \dfrac{dI_{Lb}}{dt} = -\dfrac{R_{Lb}}{L_b} I_{Lb} + \dfrac{V_{pv}}{L_b} \\ \dfrac{dV_{dc\_bus}}{dt} = \dfrac{1}{C_{dc}} I_{inv} \\ \dfrac{dI_{inv}}{dt} = -\dfrac{1}{L_{inv}} V_{dc\_bus} - \dfrac{R_{Linv}}{L_{inv}} I_{inv} - \dfrac{V_g}{L_{inv}} \end{cases} \tag{9}$$

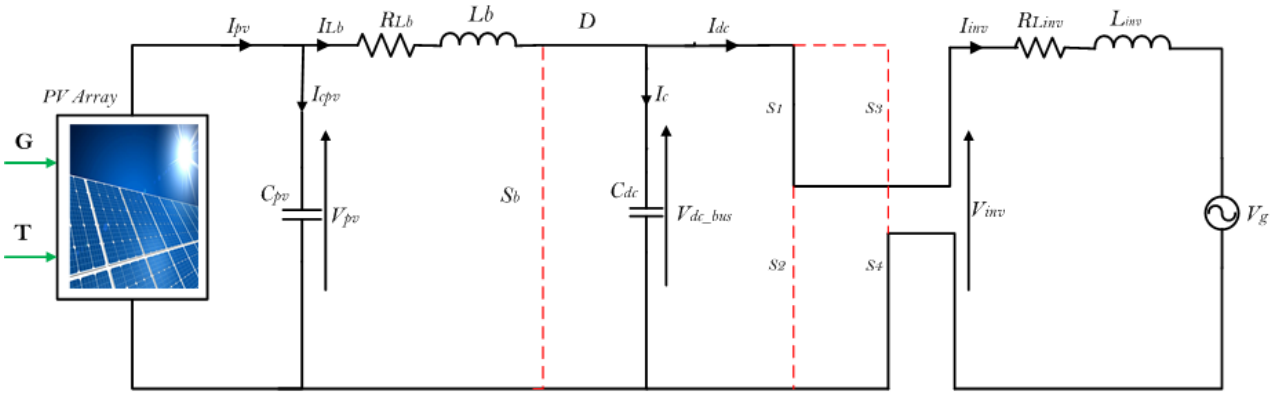

Figure 4. *Energy transfer phase 1.*

$$\begin{cases} \dfrac{dI_{Lb}}{dt} = -\dfrac{R_{Lb}}{L_b} I_{Lb} - \dfrac{1}{L_b} V_{bus\_dc} + \dfrac{V_{pv}}{L_b} \\ \dfrac{dV_{dc\_bus}}{dt} = \dfrac{1}{C_{dc}} I_{Lb} - \dfrac{1}{C_{dc}} I_{inv} \\ \dfrac{dI_{inv}}{dt} = \dfrac{1}{L_{inv}} V_{dc\_bus} - \dfrac{R_{Linv}}{L_{inv}} I_{inv} - \dfrac{V_g}{L_{inv}} \end{cases} \tag{10}$$

Conduction sequence 4: Sb opened and D on (converter side μ_1=0); S_1, S_4 open and S_2, S_3 closed (inverter side μ_2=0)

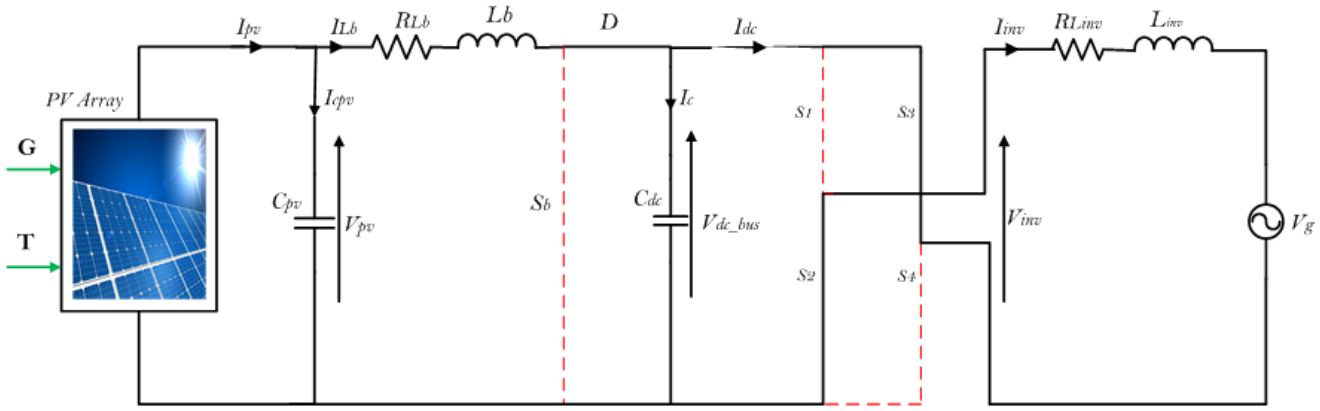

Figure 5. *Energy transfer phase 2.*

$$\begin{cases} \dfrac{dI_{Lb}}{dt} = -\dfrac{R_{Lb}}{L_b} I_{Lb} - \dfrac{1}{L_b} V_{dc\_bus} + \dfrac{V_{pv}}{L_b} \\ \dfrac{dV_{dc\_bus}}{dt} = \dfrac{1}{C_{dc}} I_{Lb} + \dfrac{1}{C_{dc}} I_{inv} \\ \dfrac{dI_{inv}}{dt} = -\dfrac{1}{L_{inv}} V_{dc\_bus} - \dfrac{R_{Linv}}{L_{inv}} I_{inv} - \dfrac{V_g}{L_{inv}} \end{cases} \tag{11}$$

Average dynamic model

By combining systems (8), (9), (10), and (11), the average dynamic model of the system can be derived as follows:

$$\begin{cases} \dfrac{dI_{Lb}}{dt} = -\dfrac{R_{Lb}}{L_b} I_{Lb} - \dfrac{(1-\mu_1)}{L_b} V_{dc\_bus} + \dfrac{V_{pv}}{L_b} \\ \dfrac{dV_{dc\_bus}}{dt} = \dfrac{(1-\mu_1)}{C_{dc}} I_{Lb} - \dfrac{(2\mu_2 - 1)}{C_{dc}} I_{inv} \\ \dfrac{dI_{inv}}{dt} = \dfrac{(2\mu_2 - 1)}{L_{inv}} V_{dc\_bus} - \dfrac{R_{Linv}}{L_{inv}} I_{inv} - \dfrac{V_g}{L_{inv}} \end{cases} \tag{12}$$

With $\mu_1, \mu_2 \in [0,1]$

I_{Lb}, R_{Lb} and L_b are the current, internal resistance, and boost converter inductance respectively. V_{pv} is the voltage supplied by the PV module; V_{dcbus} is the DC bus voltage. I_{inv}, R_{inv}, and L_{inv} are the current, resistance, and inductance of the inverter respectively. V_g is the grid voltage; μ_1 and μ_2 are the duty cycles of the boost converter and the inverter respectively.

By setting $x_1 = I_{Lb}$; $x_2 = V_{dc\_bus}$ and $x_3 = I_{inv}$, the equation (12) is transformed as follows:

$$\begin{cases} \dot{x}_1(t) = -\dfrac{R_{Lb}}{L_b} x_1(t) - \dfrac{1}{L_b} x_2(t) + \dfrac{x_2(t)}{L_b} \mu_1 + \dfrac{V_{pv}}{L_b} \\ \dot{x}_2(t) = \dfrac{1}{C_{dc}} x_1(t) + \dfrac{1}{C_{dc}} x_3(t) - \dfrac{x_1(t)}{C_{dc}} \mu_1 - \dfrac{2x_3(t)}{C_{dc}} \mu_2 \\ \dot{x}_3(t) = -\dfrac{1}{L_{inv}} x_2(t) - \dfrac{R_{Linv}}{L_{inv}} x_3(t) + \dfrac{2x_2(t)}{L_{inv}} \mu_2 - \dfrac{V_g}{L_{inv}} \end{cases} \tag{13}$$

Equation (13) takes the form of equation (14) as:

$$\dot{x}(t) = Ax(t) + g_1(x)\mu_1 + g_2(x)\mu_2 + E_d d \tag{14}$$

With:

$$A = \begin{pmatrix} -\dfrac{R_{Lb}}{L_b} & -\dfrac{1}{L_b} & 0 \\ \dfrac{1}{C_{dc}} & 0 & \dfrac{1}{C_{dc}} \\ 0 & -\dfrac{1}{L_{inv}} & -\dfrac{R_{inv}}{L_{inv}} \end{pmatrix}; g_1 = \begin{pmatrix} \dfrac{x_2(t)}{L_b} \\ \dfrac{-x_1(t)}{C_{dc}} \\ 0 \end{pmatrix}; g_2 = \begin{pmatrix} 0 \\ \dfrac{-2x_3(t)}{C_{dc}} \\ \dfrac{2x_2(t)}{L_{inv}} \end{pmatrix}; E_d = I_{3x3}; d = \begin{pmatrix} \dfrac{V_{pv}}{L_b} \\ 0 \\ \dfrac{-V_g}{L_{inv}} \end{pmatrix}$$

Equation (14) represents the nonlinear dynamic model of the system.

3. Construction of the Studied Observer

3.1. Model of Dynamic Nominal state

By setting the state, reference, and output variables as follows:

$x_{Lb\_ref} = x_{1\_ref}(t); V_{dc\_bus\_ref} = x_{2\_ref}(t); I_{inv\_ref} = x_{3\_ref}(t)$; $x(t) = \begin{bmatrix} I_{Lb}(t) & V_{dc\_bus}(t) & I_{inv}(t) \end{bmatrix}^T$ and $y(t) = \begin{bmatrix} I_{Lb} & V_{dc\_bus} & I_{inv} \end{bmatrix}^T$; equation (13) can be written as:

$$\begin{cases} \dfrac{dx_1}{dt} = -\dfrac{R_{Lb}}{L_b}x_1(t) - \dfrac{1}{L_b}x_2(t) + \dfrac{x_{2\_ref}(t)}{L_b}\mu_1 + \left[\dfrac{V_{pv}}{L_b} + \left(\dfrac{x_2(t)}{L_b} - \dfrac{x_{2\_ref}(t)}{L_b}\right)\mu_1\right] \\ \dfrac{dx_2}{dt} = \dfrac{1}{C_{dc}}x_1(t) + \dfrac{1}{C_{dc}}x_3(t) - \dfrac{x_{1\_ref}(t)}{C_{dc}}\mu_1 - \dfrac{2x_{3\_ref}(t)}{C_{dc}}\mu_2 + \left[\left(-\dfrac{x_1(t)}{C_{dc}} + \dfrac{x_{1\_ref}(t)}{C_{dc}}\right)\mu_1 + \left(-\dfrac{2x_3}{C_{dc}} + \dfrac{2x_{3\_ref}(t)}{C_{dc}}\right)\mu_2\right] \\ \dfrac{dx_3}{dt} = -\dfrac{1}{L_{inv}}x_2(t) - \dfrac{R_{Linv}}{L_{inv}}x_3(t) + \dfrac{2x_{2\_ref}(t)}{L_{inv}}\mu_2 + \left[-\dfrac{V_g}{L_{inv}} + \left(\dfrac{2x_2(t)}{L_{inv}} - \dfrac{2x_{2\_ref}(t)}{L_{inv}}\right)\mu_2\right] \end{cases} \quad (15)$$

Considering $U_1 = \begin{pmatrix} U_{11} \\ U_{12} \\ U_{13} \end{pmatrix} = \begin{pmatrix} x_{2\_ref}(t).\mu_1 \\ x_{1\_ref}(t).\mu_1 \\ 0 \end{pmatrix}$ and $U_2 = \begin{pmatrix} U_{21} \\ U_{22} \\ U_{23} \end{pmatrix} = \begin{pmatrix} 0 \\ x_{3\_ref}(t).\mu_2 \\ x_{2\_ref}(t).\mu_2 \end{pmatrix}$ as the system controls (boost converter and inverter controls respectively), and $d(x,u,t) = \begin{pmatrix} d_1(x,u,t) \\ d_2(x,u,t) \\ d_3(x,u,t) \end{pmatrix} = \begin{pmatrix} \left(\dfrac{V_{pv}}{L_b} + \left(\dfrac{x_2(t)}{L_b} - \dfrac{x_{2\_ref}(t)}{Lb}\right)\mu_1\right) \\ \left(-\dfrac{x_1(t)}{C_{dc}} + \dfrac{x_{1\_ref}(t)}{C_{dc}}\right)\mu_1 + \left(-\dfrac{2x_3}{C_{dc}} + \dfrac{2x_{3\_ref}(t)}{C_{dc}}\right)\mu_2 \\ -\dfrac{V_g}{L_{inv}} + \left(\dfrac{2x_2(t)}{L_{inv}} - \dfrac{2x_{2\_ref}(t)}{L_{inv}}\right)\mu_2 \end{pmatrix}$, a nonlinear function representing the nonlinearity of the system and the parts likely to be disturbed, the equation (15) becomes:

$$\begin{cases} \dot{x}_1(t) = -\dfrac{R_{Lb}}{L_b}x_1(t) - \dfrac{1}{L_b}x_2(t) + \dfrac{1}{L_b}U_{11}(t) + d_1(x,u,t) \\ \dot{x}_2(t) = \dfrac{1}{C_{dc}}x_1(t) + \dfrac{1}{C_{dc}}x_3(t) - \dfrac{1}{C_{dc}}U_{12}(t) - \dfrac{1}{C_{dc}}U_{22}(t) + d_2(x,u,t) \\ \dot{x}_3(t) = -\dfrac{1}{L_{inv}}x_2(t) - \dfrac{R_{Linv}}{L_{inv}}x_3(t) + \dfrac{1}{L_{inv}}U_{23}(t) + d_3(x,u,t) \end{cases} \quad (16)$$

1) The disturbances d_1 are influenced by the parameters V_{pv}, L_b, the state x_2 and the duty cycle μ_1
2) The disturbances d_2 are influenced by the parameters C_{dc}, the state x_1, x_3 and the duty cycle μ_1, μ_2
3) The disturbances d_3 are influenced by the parameters V_g, L_{inv}, the state x_2 and the duty cycle μ_2

The state space representation of equation (14) can be written as:

$$\begin{cases} \dot{x}(t) = Ax(t) + B_1u_1(t) + B_2u_2(t) + E_d d(t,x,u) \\ y(t) = Cx(t) + Du(t) \end{cases} \quad (17)$$

By identification with equation (15), the following matrices are obtained:

$$A=\begin{pmatrix} -\frac{R_{Lb}}{L_b} & -\frac{1}{L_b} & 0 \\ \frac{1}{C_{dc}} & 0 & \frac{1}{C_{dc}} \\ 0 & -\frac{1}{L_{inv}} & -\frac{R_{inv}}{L_{inv}} \end{pmatrix}; B_1=\begin{pmatrix} \frac{1}{L_b} & 0 & 0 \\ 0 & -\frac{1}{C_{dc}} & 0 \\ 0 & 0 & 0 \end{pmatrix}; B_2=\begin{pmatrix} 0 & 0 & 0 \\ 0 & -\frac{2}{C_{dc}} & 0 \\ 0 & 0 & \frac{2}{L_{inv}} \end{pmatrix}$$

$$x(t)=\left[I_{Lb}(t)\ V_{dc\_bus}(t)\ I_{inv}(t)\right]^T;$$

$$y(t)=\left[I_{Lb}\ V_{dc\_bus}\ I_{inv}\right]^T;\ C=I_{3\times3};\ E_d=I_{3\times3};\ D=0_{3\times3}$$

Where $x\in\mathbb{R}^n$, $u\in\mathbb{R}$, $d\in\mathbb{R}^r$, $y\in\mathbb{R}^n$ are the state vector, input, external disturbance, measurable outputs respectively. A is the state matrix of the nominal system with dimension $n\times n$, B_i the control matrix of the nominal system with dimension $n\times n$, C the output matrix of the nominal system with dimension $r\times n$, E_d and D, are $n\times n$ dimension.

Controllability and Observability of the nominal system

Let $n(A)$ be the order of the matrix A, $n(A)=3$

The controllability and observability matrixes are obtained as follows:

$$rank(A_0)=rank\left(\left[B\quad AB\quad AB^2\right]\right)=3=n(A) \tag{18}$$

$$rank(C_0)=rank\left(\left[C\quad CA\quad CA^2\right]^T\right)=3=n(A) \tag{19}$$

For $L_b>0$; $C_{dc}>0$ and $L_{inv}>0$, the controllability matrix A_0 and the observability matrix C_0 are full rank. This means that the nominal system is controllable and observable, and therefore stable.

3.2. Model of Extended State System

By adding the extended variable $x_{n+i}=d_i=f(x,d(t),t)$ to linearize the system (17), the extended state system is written as:

$$\begin{cases}\dot{x}_e(t)=A_e x_e(t)+B_{e1}u_1(t)+B_{e2}u_2(t)+Eh(t)\\ y_e(t)=C_e x_e(t)\end{cases} \tag{20}$$

Let us make a change of the variables as follows:

$$\begin{cases}x_4=d_1(t)\\ x_5=d_2(t)\\ x_6=d_3(t)\end{cases};\ \begin{cases}h_1=\dot{d}_1(t)\\ h_2=\dot{d}_2(t)\\ h_3=\dot{d}_3(t)\end{cases};\ h(t)=\left[h_1(t)\quad h_2(t)\quad h_3(t)\right]^T$$

$$x_e(t)=\left[I_{Lb}(t)\ V_{dc\_bus}(t)\ I_{inv}(t)\ d_1(t)\ d_2(t)\ d_3(t)\right]^T;$$

$$x_e(t)=\left[x_1(t)\quad x_2(t)\quad x_3(t)\quad x_4(t)\quad x_5(t)\quad x_6(t)\right]^T;$$

The matrices derived from the equation (20) are:

$$A_e=\begin{pmatrix} -\frac{R_{LB}}{L_b} & -\frac{1}{L_b} & 0 & 1 & 0 & 0 \\ \frac{1}{C_{dc}} & 0 & 0 & 0 & 1 & 0 \\ 0 & -\frac{1}{L_{inv}} & -\frac{R_{inv}}{L_{inv}} & 0 & 0 & 1 \\ 0 & 0 & 0 & 0 & 0 & 0 \\ 0 & 0 & 0 & 0 & 0 & 0 \\ 0 & 0 & 0 & 0 & 0 & 0 \end{pmatrix};\ B_{e1}=\begin{pmatrix} \frac{1}{L_b} & 0 & 0 \\ 0 & -\frac{1}{C_{dc}} & 0 \\ 0 & 0 & 0 \\ 0 & 0 & 0 \\ 0 & 0 & 0 \\ 0 & 0 & 0 \end{pmatrix};\ B_{e2}=\begin{pmatrix} 0 & 0 & 0 \\ 0 & -\frac{2}{C_{dc}} & 0 \\ 0 & 0 & \frac{2}{L_{inv}} \\ 0 & 0 & 0 \\ 0 & 0 & 0 \\ 0 & 0 & 0 \end{pmatrix}$$

$$C_e=\left[C\ 0_{3x3}\right]^T=\begin{pmatrix} 1 & 0 & 0 \\ 0 & 1 & 0 \\ 0 & 0 & 1 \\ 0 & 0 & 0 \\ 0 & 0 & 0 \\ 0 & 0 & 0 \end{pmatrix};\ E=\begin{pmatrix} 0 & 0 & 0 \\ 0 & 0 & 0 \\ 0 & 0 & 0 \\ 1 & 0 & 0 \\ 0 & 1 & 0 \\ 0 & 0 & 1 \end{pmatrix}$$

Controllability and Observability of the extended system

Let $n(A_e)$ be the order of the matrix A_e, $n(A_e)=6$

$$rank(con)=rank\left(\left[B_e \quad A_eB_e \quad A_eB_e^{\,2} \; A_eB_e^{\,3} \quad A_eB_e^{\,4} \quad A_eB_e^{\,5}\right]\right)=3 \tag{21}$$

$$rank(obs)=rank\left(\left[C_e \quad C_eA_e \quad C_eA_e^{\,2} \; C_eA_e^{\,3} \quad C_eA_e^{\,4} \quad C_eA_e^{\,5}\right]^T\right)=6 \tag{22}$$

The $rank(obs)$ is the observability matrix rank and $rank(con)$ is the controllability matrix rank of the extended system. It's verified that $rank(obs)=n(A_e)$ and $rank(con)\neq n(A_e)$

This allows us to conclude that the extended system is observable and partially controllable for the nominal states. However, it is not controllable for the extended states. This could be because perturbations are difficult, if not impossible to control.

3.3. Generalized Extended State Observer Design

From the preceding extended state model, the generalized extended state observer is designed as follows:

$$\begin{cases}\dot{\hat{x}}_e(t)=A_e\hat{x}_e(t)+B_{e1}u_1(t)+B_{e2}u_2(t)+L(y-\hat{y}_e)\\ \hat{y}_e(t)=C_e\hat{x}_e(t)\end{cases} \tag{23}$$

Where

$\hat{x}_e(t)=\left[\left(\hat{x}(t)\right)^T \quad \left(\hat{d}(t)\right)^T\right]^T=\left[\hat{I}_{Lb}(t) \; \hat{V}_{dc\_bus}(t) \; \hat{I}_{inv}(t) \; \hat{d}_1(t) \; \hat{d}_2(t) \; \hat{d}_3(t)\right]^T$ are the estimated state variables.

$L\in\mathbb{R}^{6x3}$ is the extended state observer gain to be dimensioned.

3.3.1. Control Low

Assuming that the three nominal states of the system are observable, to mitigate the disturbances of the system in steady state, the usual control is proposed as [45]:

$$u(t)=\bar{u}_0(t)+K_x\hat{x}(t)+K_d\hat{d}(t) \tag{24}$$

Where $\bar{u}_0(t)=\ell^{-1}\left(C(s)E(s)\right)$, $C(s)$ is the internal model of reference input *r(t)*, $E(s)$ is the Laplace transform of tracking error *e(t)* = *r(t)* - *y(t)*; ℓ^{-1} the inverse Laplace transform; K_x is the state-feedback control gain; and K_d is the disturbance compensation gain.

$$e(t)=r(t)-y(t)=\left[I_{Lb\_ref}(t) \; V_{dc\_bus\_ref}(t) \; I_{inv\_ref}(t)\right]^T-\left[I_{Lb}(t) \; V_{dc\_bus}(t) \; I_{inv}(t)\right]^T \tag{25}$$

In this study, the two commands of our system are written as follows:

$$\begin{cases}u_1(t)=\bar{u}_{01}(t)+K_{x1}\hat{x}_1(t)+K_{x2}\hat{x}_2(t)+K_{d1}\hat{d}_1(t)+K_{d2}\hat{d}_2(t)\\ u_2(t)=\bar{u}_{02}(t)+K_{x2}\hat{x}_2(t)+K_{x3}\hat{x}_3(t)+K_{d2}\hat{d}_2(t)+K_{d3}\hat{d}_3(t)\end{cases} \tag{26}$$

Let us set:

$K'_x=\left[K_{x1} \quad K_{x2}\right]$; $K''_x=\left[K_{x2} \quad K_{x3}\right]$;

$K'_d=\left[K_{d1} \quad K_{d2}\right]$; $K''_d=\left[K_{d2} \quad K_{d3}\right]$;

$\hat{x}'(t)=\left(\hat{x}_1(t) \quad \hat{x}_2(t)\right)$; $\hat{x}''(t)=\left(\hat{x}_2(t) \quad \hat{x}_3(t)\right)$;

$\hat{d}'(t)=\left(\hat{d}_1(t) \quad \hat{d}_2(t)\right)$; $\hat{d}''(t)=\left(\hat{d}_2(t) \quad \hat{d}_3(t)\right)$

Equation (26) becomes:

$$\begin{cases}u_1(t)=\bar{u}_{01}(t)+K'_x\hat{x}'(t)+K'_d\hat{d}'(t)\\ u_2(t)=\bar{u}_{02}(t)+K''_x\hat{x}''(t)+K''_d\hat{d}''(t)\end{cases} \tag{27}$$

Figure 6 shows the configuration of the proposed GESO system.

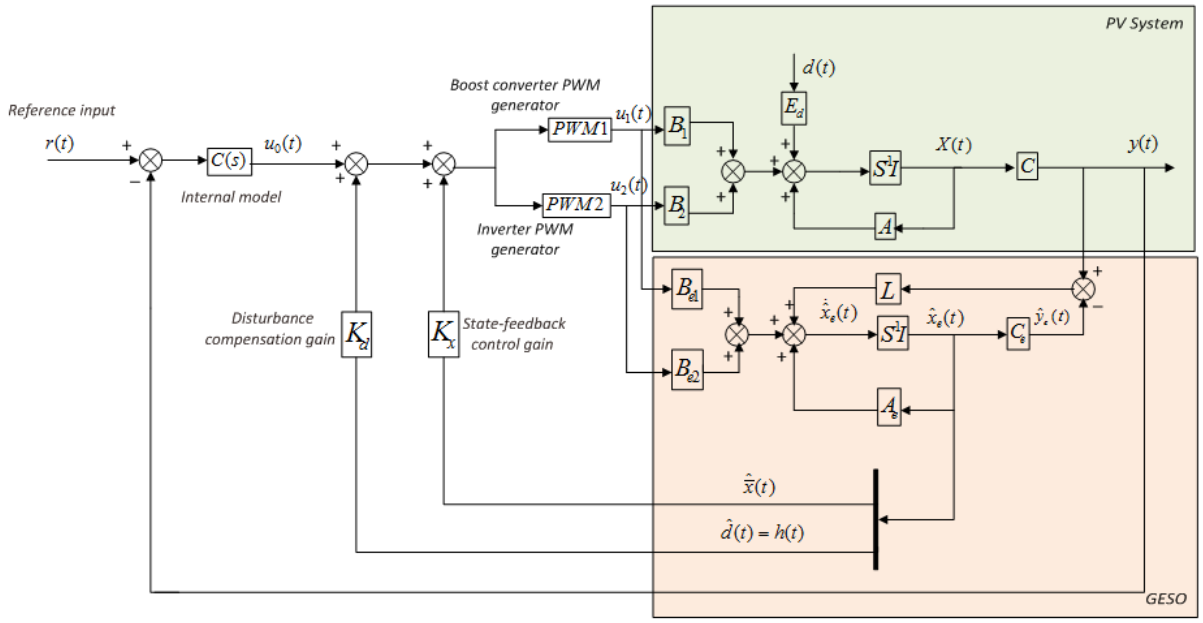

Figure 6. *Configuration of the proposed GESO-based control system.*

3.3.2. System Stability Analysis

Assumption: Disturbances and their derivatives are bounded, and have constant values in steady state. $\lim_{t\to\infty} d_i(t,x,u) \approx D_i$ et $\lim_{t\to\infty} \dot{d}_i(t) = \lim_{t\to\infty} h(t) \approx 0$; D_i is a constant and $i = 1,2,3$ [25].

The estimation errors of the state variables and disturbances are defined as follows:

$$\varepsilon = x_e - \hat{x}_e = \begin{bmatrix} i_{Lb}(t) - \hat{i}_{Lb}(t) \\ v_{dc-bus}(t) - \hat{v}_{dc-bus}(t) \\ i_{inv}(t) - \hat{i}_{inv}(t) \\ d_1(t) - \hat{d}_1(t) \\ d_2(t) - \hat{d}_2(t) \\ d_3(t) - \hat{d}_3(t) \end{bmatrix} \tag{28}$$

From the extended state system (20) and the generalized extended state observer (23), the dynamic state equation of the error is given by:

$$\dot{\varepsilon}(t) = \left(A_e - LC_e\right)\varepsilon(t) + Eh(t) \tag{29}$$

Lemma: Assuming that the Extended State Observer gain vector L is chosen so that $\left(A_e - LC_e\right)$ is Hurwitz matrix, and then the observer error $\varepsilon(t)$ is bounded for any bounded disturbance $d_i(t)$ [25].

From Lemma 1, it can be concluded that the closed-loop system (23) is bounded-input–bounded-output stable for any bounded d(t) and h(t) if Kx and L are well-defined.

Theorem 1: Suppose that the *Assumption* is satisfied. The stability of system (23) is guaranteed if the ESO gain L and the state feedback control gain K_x are chosen such that matrices $\left(A_e - LC_e\right)$ and $\left(A + BK_x\right)$ are Hurwitz [25].

Theorem 2: The disturbance compensation gain K_d is no longer available since $C\left(A + BK_x\right)^{-1} B$ is possible noninvertible or even not a square matrix [25].

Considering theorem 2, assuming that $C\left(A + BK_x\right)^{-1} B$ is invertible, then the disturbance compensation gain K_d takes the form:

$$K_d = -\left[C\left(A + BK_x\right)^{-1} B\right]^{-1} C\left(A + BK_x\right)^{-1} E_d \tag{30}$$

Theorem 3: Suppose that Assumption 1 is satisfied. If the following conditions are satisfied [36]:

1) Matrix $\left(A_e - LC_e\right)$ is Hurwitz;

2) Matrix $\left(A + BK_x\right)$ is Hurwitz;

3) Matrix $C\left(A + BK_x\right)^{-1} B$ is invertible

According to the control law (24), the disturbance d(x, t) can then be attenuated from the output channel in a the steady state.

Remark: The influence of disturbances on the system state may not be completely eliminated [36]. In the case studied, one of the main objectives is to eliminate the effects of any disturbance from the output channel. Theorem 3 gives the necessary conditions for the closed-loop GESO to ensure stability and attenuation of disturbances from the output channel in the steady state.

3.3.3. Active Disturbance Rejection Analysis

Substituting $\varepsilon_x(t) = x(t) - \hat{x}(t)$; $\varepsilon_d(t) = d(t) - \hat{d}(t)$ and $u(t) = \bar{u}_0(t) + K_x\hat{x}(t) + K_d\hat{d}(t)$ into equation (17), the following equation is obtained:

$$x(t) = \left(A + BK_x\right)^{-1}\left[\dot{x}(t) - B\bar{u}_0(t) + (BK_d + E_d)\varepsilon_d(t) - (BK_d + E_d)d(t) + BK_x\varepsilon_x(t)\right] \tag{31}$$

Substituting equations (30) and (31) into equation (17), the output can be represented as:

$$y(t) = Cx(t) = C\left(A + BK_x\right)^{-1}\dot{x}(t) - C\left(A + BK_x\right)^{-1}B\bar{u}_0(t) + C\left(A + BK_x\right)^{-1}BK_x\varepsilon_x(t) \tag{32}$$

It is clear that the output of the system does not contain the distorted expression. We can therefore conclude that there is active noise suppression at the output of the system.

3.3.4. Algorithm for Designing the GESO-based PV System

Step 1: Design the observer gains L through the pole placement method, ensuring that $\left(A_e - LC_e\right)$ is Hurwitz.

Step 2: Design feedback control gain K_x by the pole placement method so that $\left(A + BK_x\right)$ is Hurwitz.

Step 3: Check if $C\left(A + BK_x\right)^{-1}B$ is inversible. If not, go to Step 2, and redesign K_x

Step 4: Calculate K_d from (30).

4. Simulation Results

4.1. Studied System Parameters

In this section, the proposed GESO-based method is applied to the system with the parameters shown in Table 1.

Table 1. *System parameters [30, 33].*

Parameter	Symbol	Value
Photovoltaic generator voltage	V_{pv}	120 V
Boost converter inductance	L_b	5 mH
Internal resistance of converter	R_{Lb}	1 Ω
Boost converter current	I_{Lb}	12 A
DC bus capacitance	C_{dc}	2.85 mF
DC bus voltage	V_{dc_bus}	240 V
Inverter inductance	L_{inv}	5.16 mH
Internal resistance of inverter	R_{inv}	1 Ω
Inverter current	I_{inv}	6 A
Grid voltage	V_g	220 V
Switching frequency	f_c	20 kHz
Sample time	t	10^{-5} S

There are three main parameters to design the GESO; the observer gain matrix L, the disturbance compensation gain K_d and the feedback control gain matrix K_x. The algorithm described in section 3.3.4 is used to determine these parameters. The most important design parameters are K_x and L [25]. They ensure the stability of the closed-loop system. They should be chosen to stabilize the error dynamics and to allow $\varepsilon(t)$ to move rapidly to zero independently of $\varepsilon(0)$ [13]. The pole placement approach allows one to parameterize the gains and analytically define the desired behaviour of the observer outputs by setting the characteristic polynomial [46]:

$$\lambda(s) = \det\left(sI - (A_e - LC_e)\right) \tag{33}$$

Where λ_i are the eigenvalues of matrix $\left(A_e - LC_e\right)$.

The nominal system (A, B) is controllable and the extended system (A_e, C_e) is observable. Matrices $\left(A + BK_x\right)$ and $\left(A_e - LC_e\right)$ are Hurwitz, the poles of both the closed-loop system and the ESO can be placed arbitrarily [25].

By choosing the pole placement as $poleA = \left[-9 \quad -6 \quad -6\right]$, the feedback control gain matrix is

$$K_x = \begin{bmatrix} -0.0040 & -0.0042 & 0.0000 \\ -0.0000 & -0.021 & -0.0020 \\ -0.0833 & -0.0122 & -0.0813 \end{bmatrix} \tag{34}$$

The Eigen values of matrix $\left(A + BK_x\right)$ are: $\left\{-9 \quad -6 \quad -6\right\}$

The real parts of the eigenvalues are negative, so the matrix $\left(A + BK_x\right)$ is Hurwitz. The nominal system is therefore stable. The disturbance compensation gain K_d is obtained as follows:

$$K_d = \begin{bmatrix} -0.0000 & -0.0000 & -0.0000 \\ 0.0000 & 0.0000 & -0.0000 \\ 0.0000 & 0.0024 & 0.0000 \end{bmatrix} \quad (35)$$

By choosing $poleA_e = [-70 \quad -315 \quad -475 \quad -2160 \quad -3150 \quad -6074]$; observer gain matrix L is obtained as:

$$L = 10^7 * \begin{bmatrix} 0.0009 & -0.0000 & 0.0000 \\ 0.0000 & 0.0001 & 0.0000 \\ 0.0000 & -0.0000 & 0.0002 \\ 1.9133 & 0.0000 & 0.0000 \\ 0.0000 & 0.0150 & 0.0000 \\ 0.0000 & 0.0000 & 0.0151 \end{bmatrix} \quad (36)$$

The eigenvalues of $(A_e - LC_e)$ are: $\{-6074 \quad -3150 \quad -2160 \quad -70 \quad -315 \quad -475\}$.

These values are completely negative, so matrix $(A_e - LC_e)$ is Hurwitz ensuring the stability of GESO.

4.2. States and Disturbances Estimation Results

The response curves of the real and estimated states I_{Lb}, V_{dc_bus}, and I_{inv}, and their estimation errors are shown in Figures 7-9. The estimated curves converge correctly to the real curves as can be seen from these figures and the estimation errors of GESO converge to zero.

In Figure 8, the small oscillations observed in the V_{dc_bus} response curve would be caused by the current term Iinv in the expression of the DC bus voltage equation.

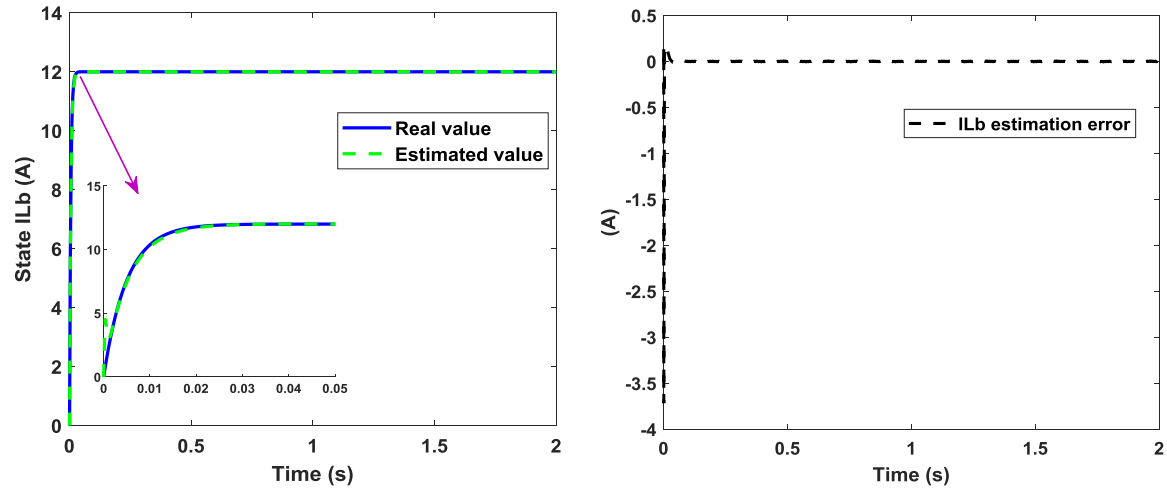

(a) (b)

Figure 7. *Response curves of the real and estimated boost converter inductance current I_{Lb} (a) and estimation error (b).*

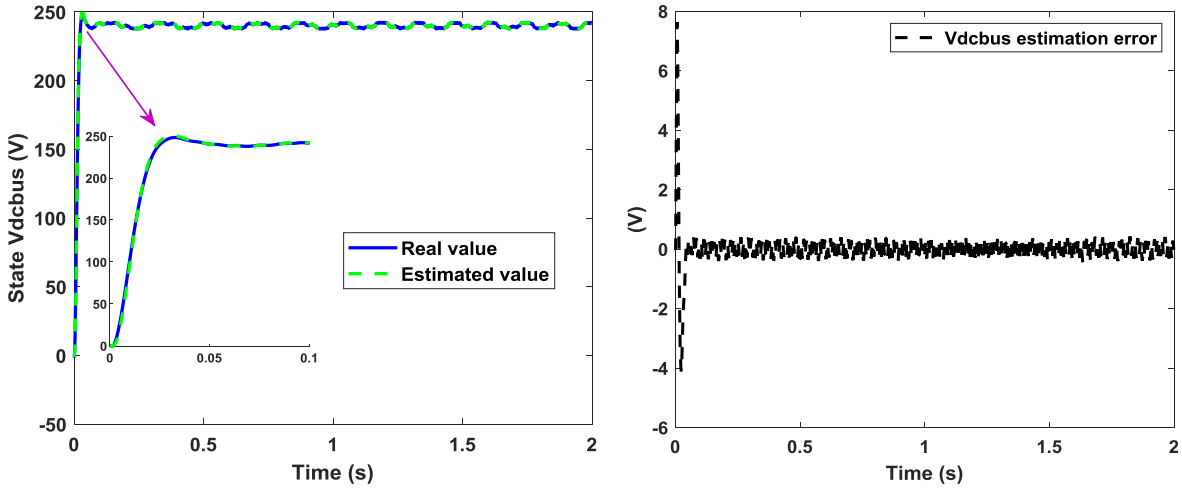

(a) (b)

Figure 8. *Response curves of the real and estimated DC bus voltage V_{dc_bus} (a) and the estimation error (b).*

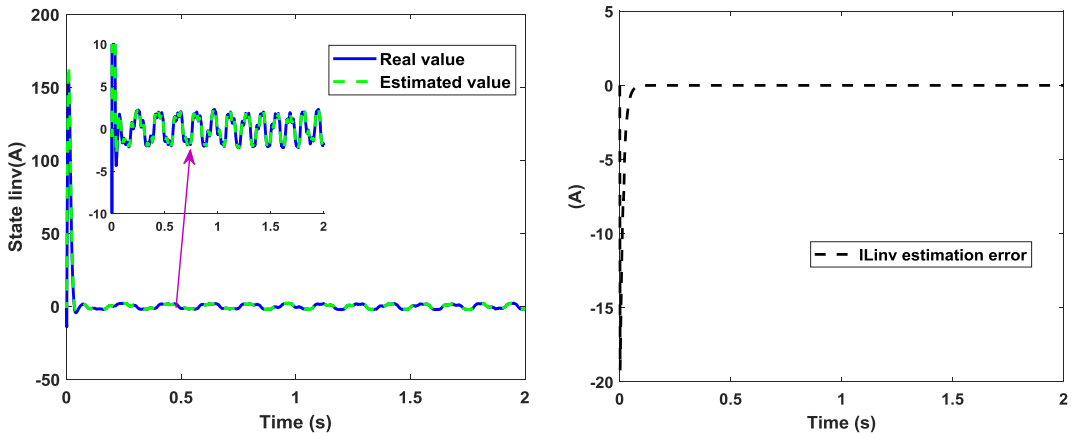

(a) (b)

Figure 9. *Response curves of the real and estimated inverter current I_{inv} (a) and estimation error (b).*

Figures 10-12 show the response curves of the real and estimated disturbances d_1, d_2, and d_3 and their estimation errors. It can be seen that the estimated curves correctly converge to the real curves and the estimation errors of GESO converge to zero for all disturbances.

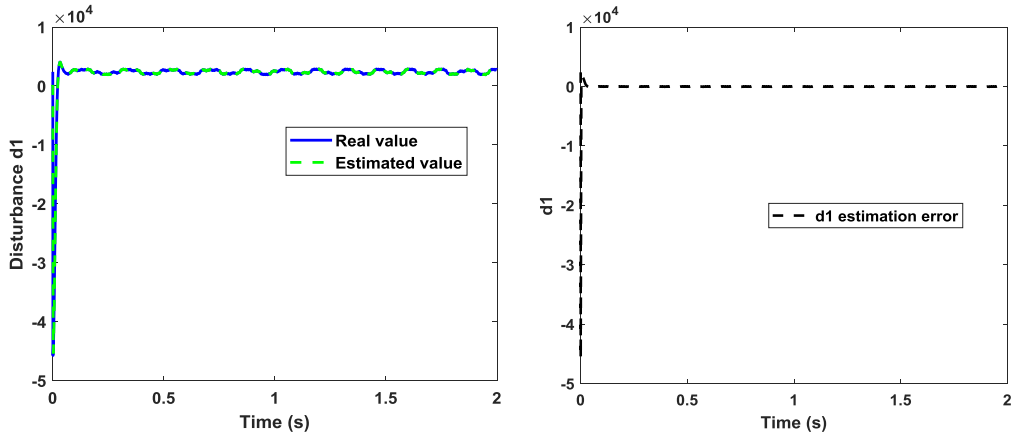

(a) (b)

Figure 10. *Real and estimated disturbance d_1 curves (a) and estimation error (b).*

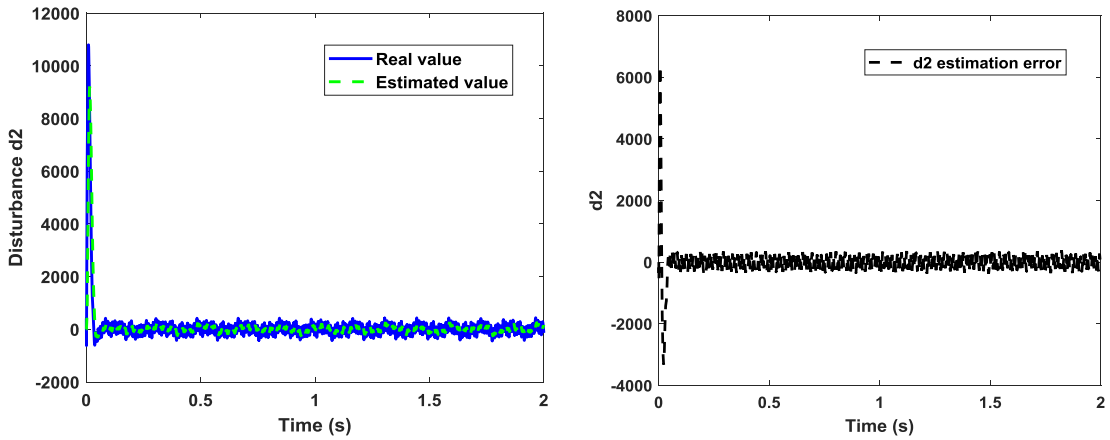

(a) (b)

Figure 11. *Real and estimated disturbance d_2 curves (a) and estimation error (b).*

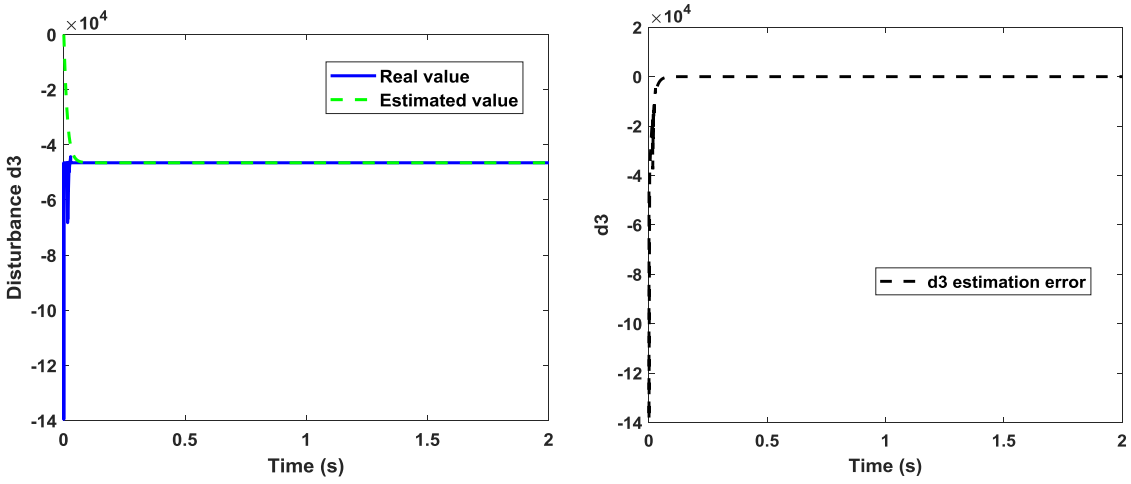

(a) (b)

Figure 12. *Real and estimated disturbance d_3 curves (a) and estimation error (b).*

As shown in Figures 7-12, the GESO can estimate the states and disturbances timely and accurately.

4.3. Test of GESO Robustness

The GESO is subjected to PV and grid voltage variations in this section. The aim is to test the robustness of the estimator to see if these external disturbances have impacts on the estimation of the system states.

4.3.1. GESO Subjected to Photovoltaic Voltage (V_{pv}) Variation

In this work, we assume that the voltage variation is due to partial shading. To this end, we have based our analysis on the work conducted by the author [44]. This work deals with the effect of partial shading on the performance of PV modules operating in the Sudanese-Sahelian climate of Cameroon. The voltage variation according to shading is shown in the table below.

Table 2. *The effect of shading on V_{pv} voltage.*

Nominal V_{pv} Voltage: 120 V		
Shading	**Voltage drop**	**Operating voltage**
60 %	55.78 % (66.93 V)	53.01 V
65 %	56.17 % (67.40 V)	52.60 V
70 %	56.39 % (67.66 V)	52.34 V
80 %	57.61 % (69.13 V)	50.87 V
85 %	57.83 % (69.39 V)	50.61 V
90 %	57.72 % (69.26 V)	50.74 V
Nominal V_{pv} Voltage: 120 V		
Shading	**Voltage drop**	**Operating voltage**
95 %	58.22 % (69.86 V)	50.14 V

Assume that the PV generator voltage *Vpv* changes as follows according to the shading:

$$V_{pv} = \begin{cases} 120V & for \quad t \in [0s;0.2s[\\ 53.01V & for \quad t \in [0.2s;0.4s[\\ 50.87V & for \quad t \in [0.4s;0.6s[\\ 53.01V & for \quad t \in [0.6s;1s[\\ 120V & for \quad t \in [1s;1.2s[\\ 53.01V & for \quad t \in [1.2s;1.4s[\\ 52.60V & for \quad t \in [1.4s;1.6s[\\ 120V & for \quad t \in [1.6s;1.8s[\\ 50.14V & for \quad t \in [1.8s;2s[\end{cases} \tag{37}$$

According to Figures 13-15, the variation of the voltage V_{pv} due to the shading has an important effect on the current I_{Lb} while the states $V_{dc\_bus,}$ and I_{inv} remain relatively stable. Furthermore, the estimated curves correctly follow the actual curves as shown by the response curves for the three states. This means that the disturbances from the PV source do not affect the estimation of the system states. In addition, the estimation error curve in Figure 13 shows peaks of the order of 0.1 V at times of V_{pv} variation, indicating the presence of external disturbances to the system. Similarly, the presence of peaks in the estimation error curve in Figure 15 indicates the voltage drop on the PV side.

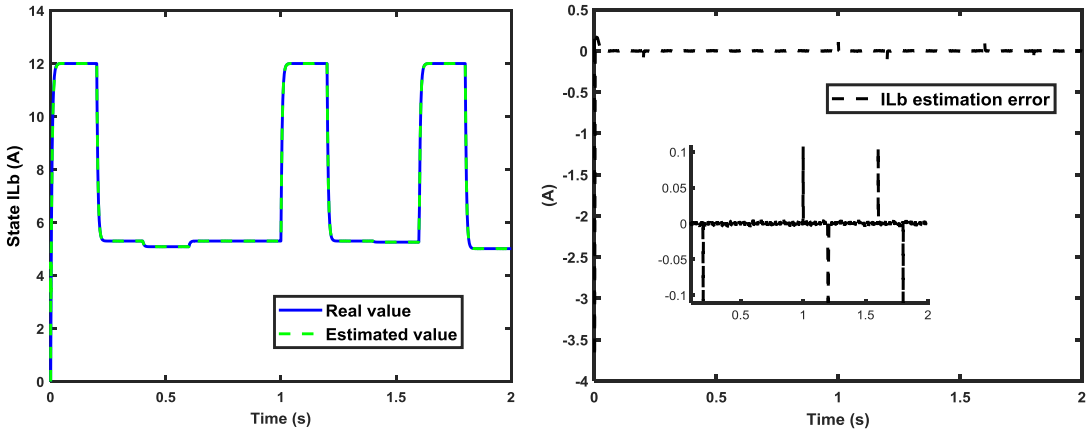

(a) (b)

Figure 13. *Response curves of the real and estimated boost converter inductance current I_{Lb} under V_{pv} variation (a) and estimation error (b).*

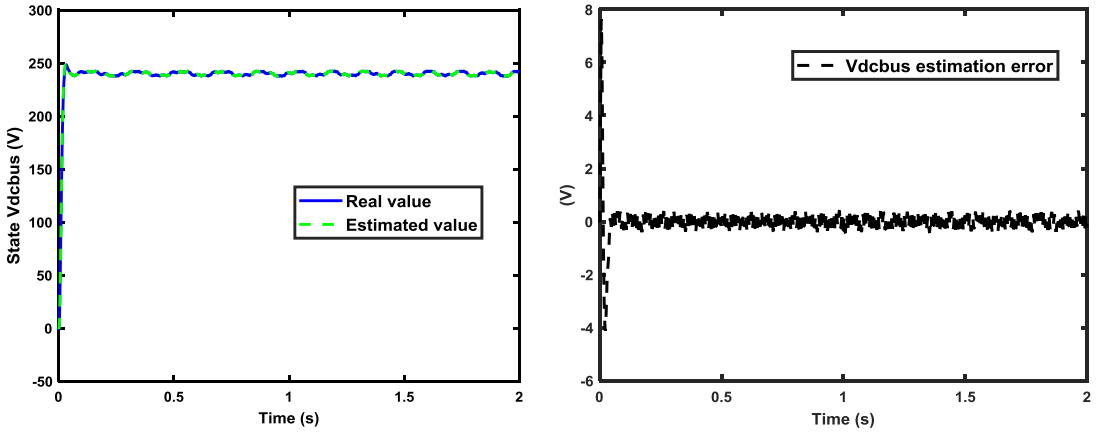

(a) (b)

Figure 14. *Response curves of the real and estimated DC bus voltage V_{dc_bus} under V_{pv} variation (a) and estimation error (b).*

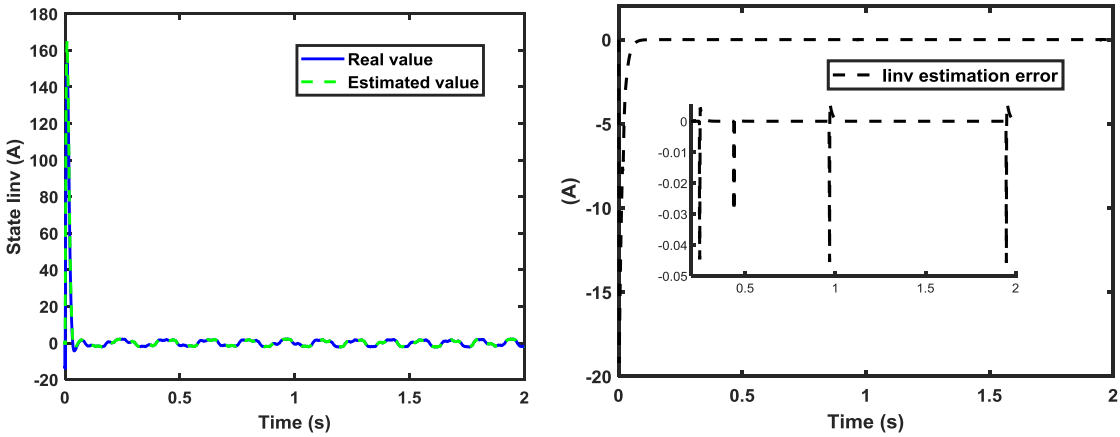

(a) (b)

Figure 15. *Response curves of the real and estimated inverter current I_{inv} under V_{pv} variation (a) and estimation error (b).*

The influence of faults from the PV source on the three modelled internal disturbances d_1, d_2 and d_3 is shown in Figures 16 and 18 by the presence of the peaks observed in the estimation error curves. As the voltage V_{pv} increases, the peaks increase, and as the voltage decreases, the peaks decrease. However, as the response curves for the three dis-

turbances show, the estimated curves correctly follow the actual curves. This demonstrates GESO's robustness in estimating disturbances.

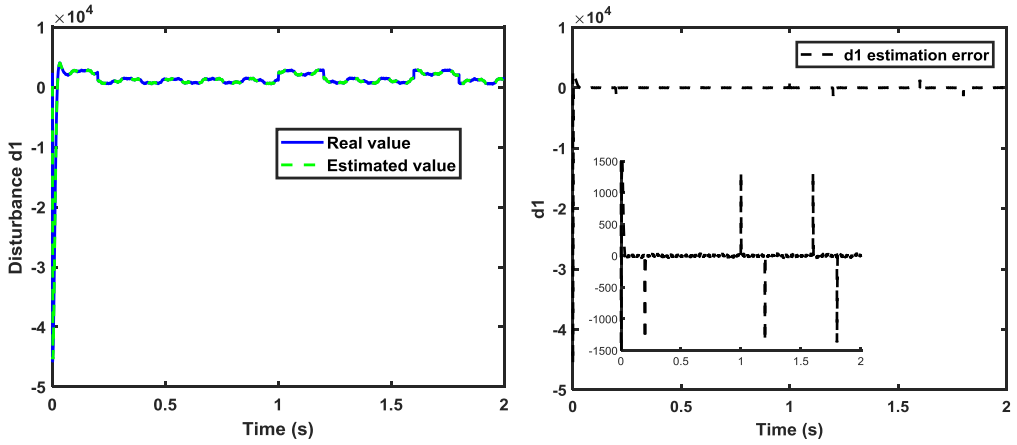

(a) (b)

Figure 16. *Real and estimated disturbance d_1 curves under V_{pv} variation (a) and estimation error (b).*

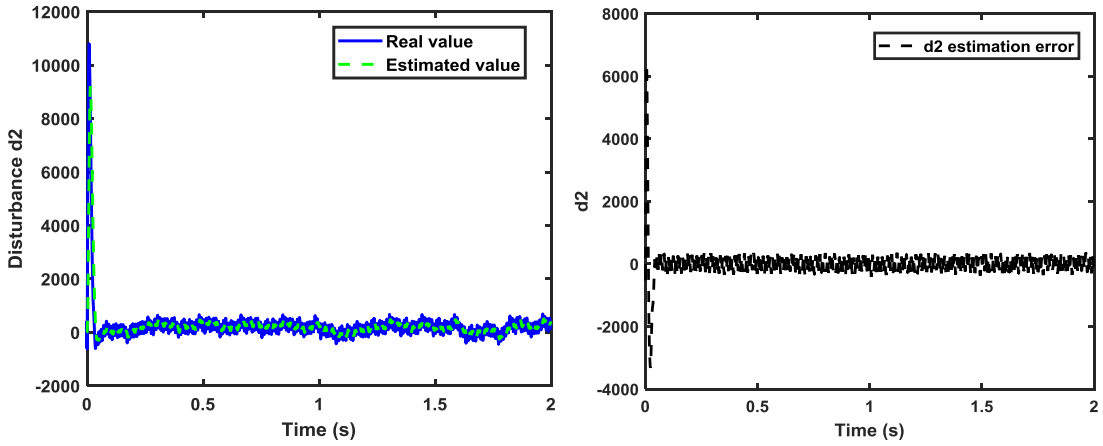

(a) (b)

Figure 17. *Real and estimated disturbance d_2 curves under V_{pv} variation (a) and estimation error (b).*

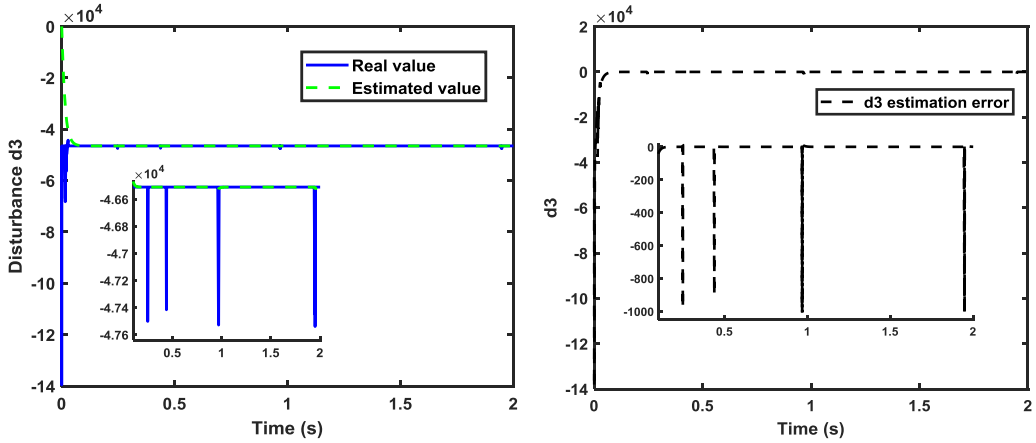

(a) (b)

Figure 18. *Real and estimated disturbance d_3 curves under V_{pv} variation (a) and estimation error (b).*

4.3.2. GESO Subjected to Grid Voltage (V_g) Variation

For a distribution network, the joule effect, overloading, line length, etc. can cause technical losses related to the operation of network equipment. In Cameroon, low-voltage distribution networks vary from 110V to 380V. In our study, assume that network disturbances cause the network voltage V_g to vary as follows:

$$V_g = \begin{cases} 240V & for \quad t \in [0s;0.2s[\\ 180V & for \quad t \in [0.2s;0.4s[\\ 160V & for \quad t \in [0.4s;0.6s[\\ 220V & for \quad t \in [0.6s;1s[\\ 280V & for \quad t \in [1s;1.2s[\\ 380V & for \quad t \in [1.2s;1.4s[\\ 240V & for \quad t \in [1.4s;1.6s[\\ 110V & for \quad t \in [1.6s;1.8s[\\ 380V & for \quad t \in [1.8s;2s[\end{cases} \tag{38}$$

As shown in Figures 19-21, GESO shows good robustness in estimating the three states I_{Lb}, V_{dc_bus} and I_{inv} when the system is subjected to grid variations. According to these figures, the presence of rising and falling peaks in the estimation error curves indicates a failure due to voltage variation on the grid side. Figure 20 also shows that the DC bus voltage varies with the grid voltage.

Furthermore, the rising and falling peaks in Figure 21 show that the current I_{inv} decreases as the grid voltage increases and it increases as the voltage decreases. This justifies the expression of the I_{inv} current in equation (12).

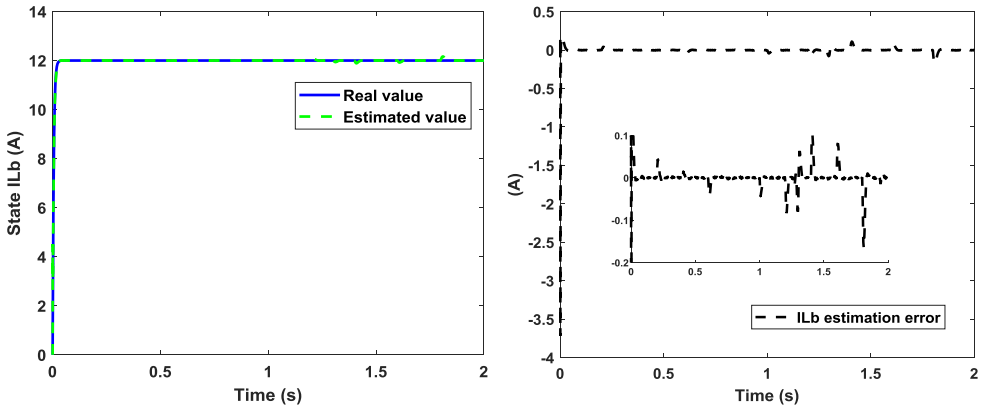

(a) (b)

Figure 19. *Response curves of the real and estimated boost converter inductance current I_{Lb} under V_g variation (a) and estimation error (b).*

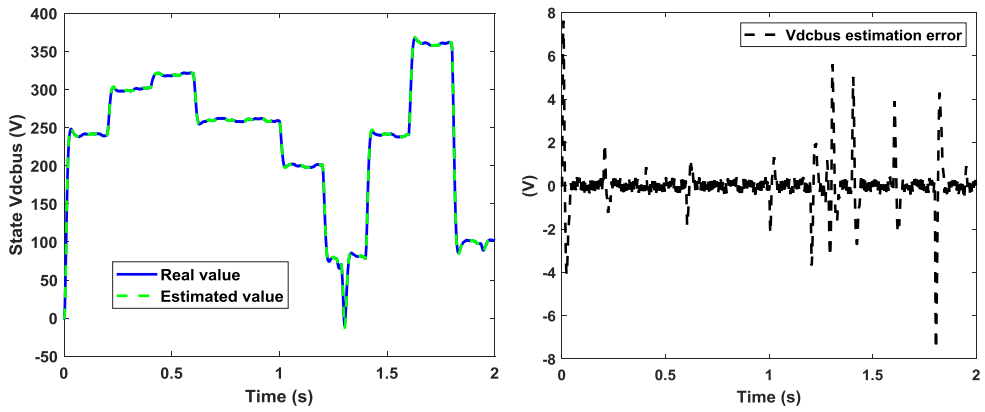

(a) (b)

Figure 20. *Response curves of the real and estimated DC voltage V_{dc_bus} under V_g variation (a) and estimation error (b).*

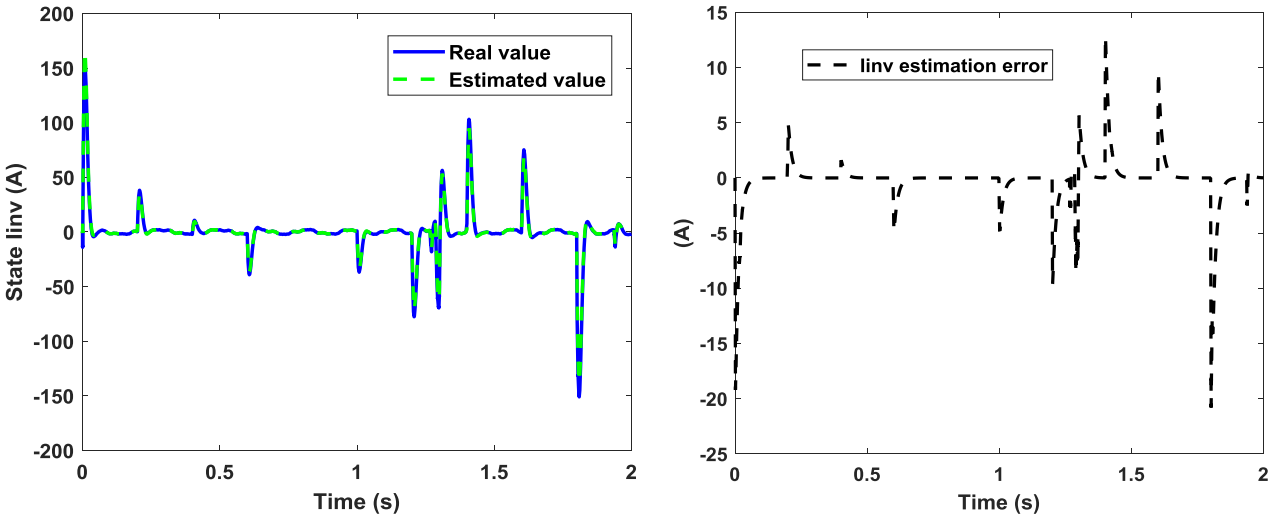

(a) (b)

Figure 21. *Response curves of the real and estimated inverter current I_{inv} under V_g variation (a) and estimation error (b).*

Figures 22-24 show that the estimated curves correctly follow the real ones, despite the disturbances coming from the grid side. The GESO shows good robustness in the estimation of the internal disturbances d_1, d_2 and d_3. In Figure 22, varying the V_g voltage varies the d_1 disturbance in the same way as it varies the DC bus voltage. This is because the disturbance d_1 model is strongly influenced by the DC bus voltage. Therefore, the peaks observed in the estimation error curve indicate the presence of an external disturbance. Figure 23 shows that the changes in disturbances d_2 due to the variation of the grid voltage are similar to those observed for the current I_{inv}, as shown by the presence of peaks in the estimation error curve. According to equation (15), the disturbance d_2 is strongly influenced by the state I_{inv}. Therefore, the forms of their modifications under the influence of the voltage V_g are practically the same. In Figure 24 the value of the disturbance d_3 increases as the voltage V_g decreases and decreases as the voltage V_g increases.

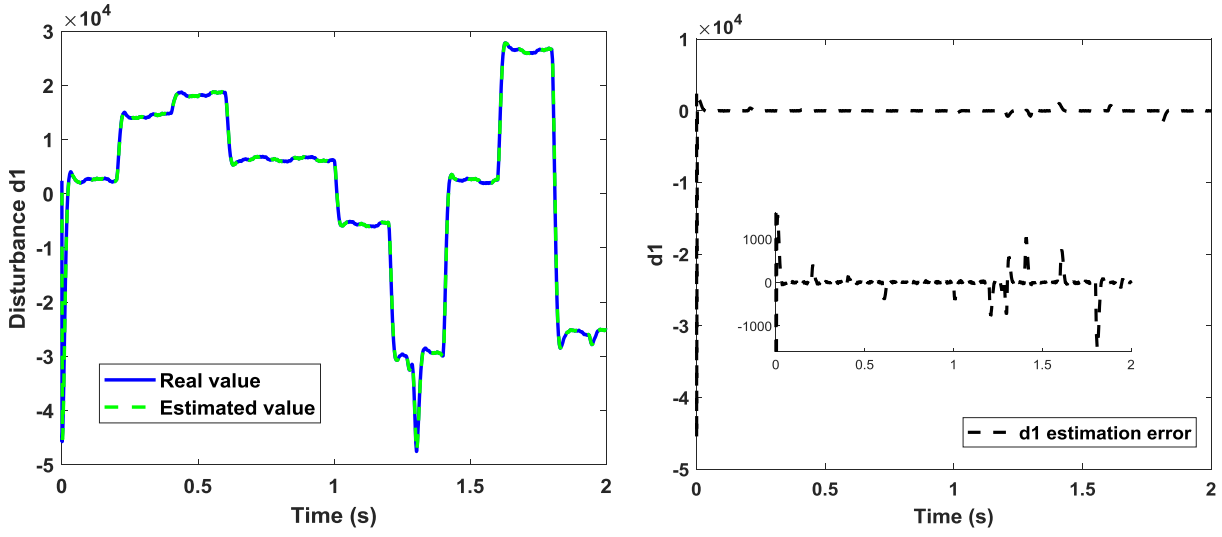

(a) (b)

Figure 22. *Real and estimated disturbance d_1 curves under V_g variation (a) and estimation error (b).*

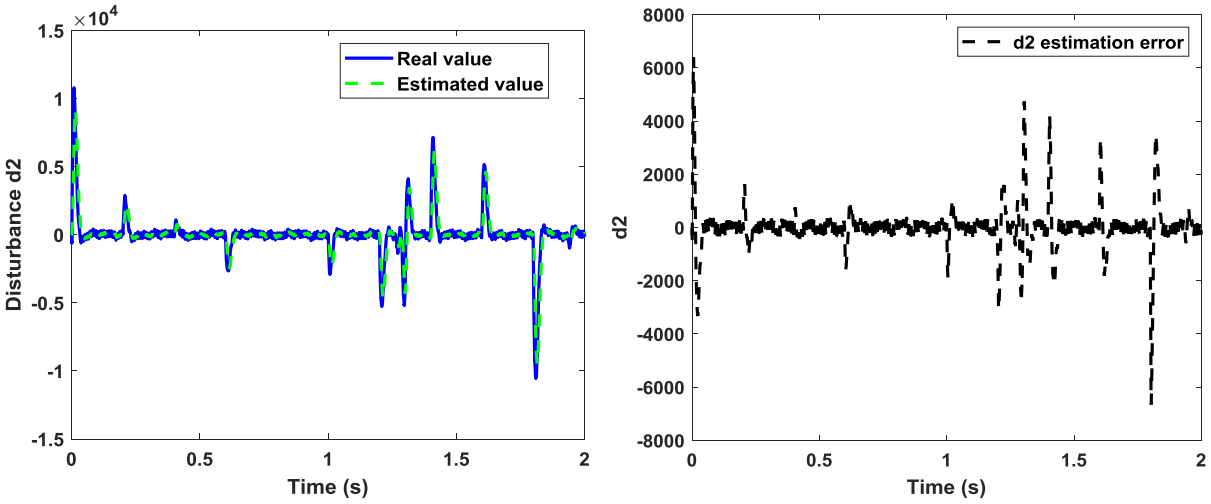

(a) (b)

Figure 23. *Real and estimated disturbance d_2 curves under V_g variation (a) and estimation error (b).*

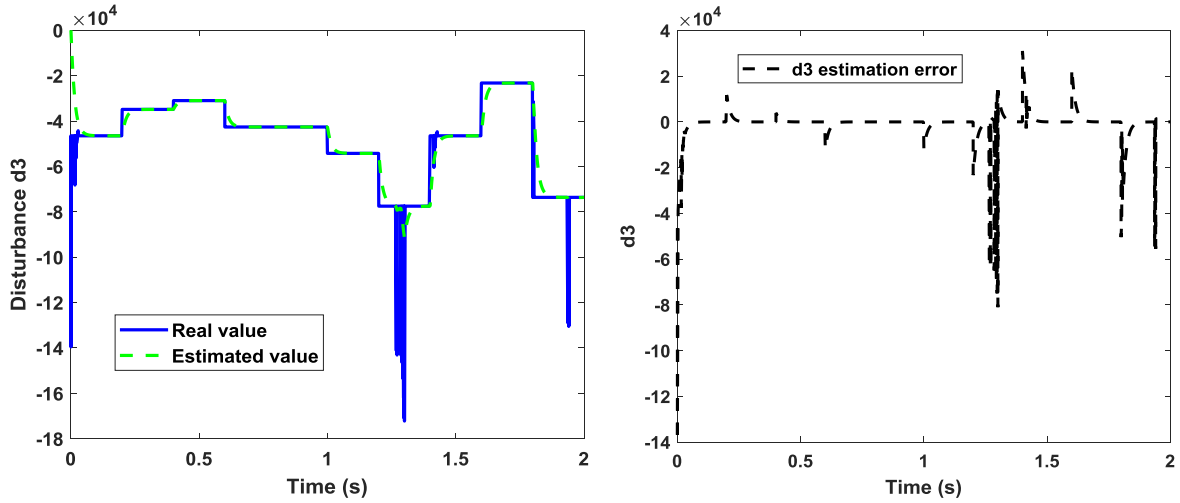

(a) (b)

Figure 24. *Real and estimated disturbance d_3 curves under V_g variation (a) and estimation error (b).*

4.4. Discussion

4.4.1. State and Disturbance Estimation Analysis

Four aspects, namely accuracy, speed, stability and robustness, underpin the proposed GESO performance. Figures 7-9 show a good estimation of the states of the I_{Lb} current, the V_{dc_bus} voltage, and the I_{inv} current by the GESO. The estimated states follow the real states in transient and steady states. The transient mode takes less than 0.02 s to estimate I_{Lb} and less than 0.05 s to estimate V_{dc_bus} and I_{Linv}.

Figures 10-12 show the estimation of the disturbances d_1, d_2, d_3. The estimated values follow the real values.

For any bounded $h(t)$ and $d(t)$, the stability of the system under the proposed GESO is guaranteed by the proper of the observer gain L and the feedback control gain K_x using the pole placement method such that A_e and $\left(A_e - LC_e\right)$ are Hurwitz matrices.

4.4.2. Analysis of Estimation Error

Figures 7-12 show the state and disturbance estimation errors. The different error curves show a convergence to zero when the system is not subject to V_{pv} and V_g fluctuations. The estimation error curves demonstrate the robustness of the control and estimator in the face of PV generator voltage and grid voltage variations. However, peaks can be observed at the variation times. This shows a slight influence of external perturbations on the GESO and indicates the presence of a fault (an external disturbance) in the system.

4.4.3. The Robustness of the Proposed GESO Under the Photovoltaic Voltage Variation

Due to the changes in atmospheric conditions (partial shading in the context of this study), the output voltage, of the PV system changes significantly [47]. As shown in Figures 13-18, the variation in V_{pv} voltage due to partial shading has a significant effect on the I_{Lb} current and a slight impact on the I_{inv} current and on disturbances d_1 and d_3. The I_{Lb} current varies proportionally to the voltage drop due to partial shading, from 55% to 59%.

In Figure 13, depending on whether the voltage is falling or rising, the current estimation error curve I_{Lb} shows peaks of the order of -0.1 A and 0.1 A at the instant of variation.

Peaks around -0.04 A are observed on the I_{inv} current estimation error curve in Figure 14. In Figure 15, the disturbance d_1 estimation error curve shows peaks of the order of 1400 and -1400 depending on the direction of the V_{pv} voltage variation. The disturbance d_3 estimation error curve shows a peak of the order of -1000 regardless of the direction of the V_{pv} voltage variation. The presence of these peaks indicates a fault outside the system. The different values indicate how much the faults affect the internal conditions of the system. However, the estimator estimates the currents and disturbances well, since the curves of the estimated values follow the curves of the real values, despite the V_{pv} variation. The proposed GESO correctly estimates the states and disturbances in the face of the PV generator faults. The states and disturbances values also return to normal when the voltage V_{pv} returns to normal. We conclude that the proposed GESO is robust to PV generator changes.

4.4.4. The Robustness of the Proposed GESO Under Grid Voltage Fluctuation

Figures 19-24 show the response of the GESO to the variation of grid voltage. The variation of the grid voltage affects the three states and the three disturbances at different levels. The I_{Lb} current remains almost stable during grid voltage fluctuation. The peaks observed in the estimation error curve indicate a fault in the system, which is reflected in the expression of the bus voltage in the state equation of I_{Lb}. The V_{dc_bus} and I_{inv} states, and the three internal disturbances modelled d_1, d_2 and d_3 are significantly affected by the grid voltage variation.

The response curves deviate from the reference at the time of the variation of the grid voltage and return to the normal ones when the network stabilizes. However, the presence of external faults does not disrupt the estimation of the states and modelled disturbances, and we observe that the estimated curves follow well the real ones. This demonstrates the robustness of the GESO in the presence of grid voltage disturbances.

5. Conclusion

As mentioned in many works in the literature, knowing the health of a system helps to guarantee its efficiency and sustainability. The state observer is one of the techniques used by several authors to estimate the state of a system. For observers applied to the PV system, many authors do not take into account the estimation of some parameters. Unlike other authors who have only taken account either the states on the DC side or the states on the AC side, the proposed method not only allows to estimate the whole states of the system but also estimate the associated disturbances. In this paper, the Generalized Extended State Observer has been used to estimate simultaneously the states and disturbances of a single-phase grid-connected photovoltaic system operating under the Sudanese-Sahelian climate of Cameroon. Over the existing observers applied to PV system, the proposed one presents the following advantages:

1) Adequate design of the nominal and extended state observer with two controls (one control on DC side and one control on AC side);
2) Simultaneously estimating of states and disturbances, considering both the DC and AC sides of the photovoltaic system;
3) A correct selection of a disturbance compensation gain, resulting from the correct pole placement, allows a good estimation of the state and disturbances, as well as the stability of the studied photovoltaic system under mismatched uncertainties;
4) Active disturbance rejection well demonstrated by the noise suppression at the system output.

The proposed adaptive GESO is robust and globally asymptotically stable, as shown by the state and disturbance estimation curves. The present work contributes to the study of observers applied to the PV system. However, the control may not work satisfactorily when the system operates under photovoltaic and grid voltage variations. It would be useful to consider the optimal control of the boost converter and the inverter, on which depend the inductance current I_{Lb}, the DC bus voltage V_{dc_bus} and the inverter current I_{inv}. Therefore, to improve the present GESO, it is necessary to strengthen the control part with a robust tool such as sliding mode control. Finally, the simulation results show that the proposed approach is quite efficient for diagnosing PV systems despite the effect of concurrent faults and unknown disturbances. The simulated results presented in this paper suggest future experimental work.

Abbreviations

V_{pv}	Photovoltaic Generator Voltage
L_b	Boost Converter Inductance
R_{Lb}	Internal Resistance of Converter
I_{Lb}	Boost Converter Current
C_{dc}	DC Bus Capacitance
V_{dc_bus}	DC Bus Voltage
L_{inv}	Inverter Inductance
R_{inv}	Internal Resistance of Inverter

I_{inv}	Inverter Current
V_g	Grid Voltage
d_1, d_2, d_3	Disturbances
K_d	Compensation Gain
L	Observer Gain
K_x	State Feedback Control Gain
A	State Matrix of the Nominal System
B_i	Control Matrix of the Nominal System
C	Output Matrix of the Nominal System
A_e	State Matrix of the Extended System
B_{ei}	Control Matrix of the Extended System
C_e	Output Matrix of the Extended System
A_0	Controllability Matrix of the Nominal System
C_0	Observability Matrix of the Nominal System
GESO	Generalized Extended State Observer
ADRC	Active Disturbance Rejection Control
PV	Photovoltaic
GADRC	Generalized Active Disturbance Rejection Control
UV	Ultraviolet
IR	Infrared
PL	Photoluminescence
EL	Electroluminescence
SMO	Sliding Mode Observer
UIO	Unknown Input Observer
LO	Learning Observers
EID	Equivalent Input Disturbance
ESO	Extended State Observer
LDUE	Linear Disturbance and Uncertainty Estimation
NDUE	Nonlinear Disturbance and Uncertainty Estimation
PID	Proportional-Integral-Derivative
LCL	Inductor (L) - Capacitor (C) - Inductor (L)
AD	Active Damping
PWM	Pulse Width Modulation
MOSFET	Metal-Oxide-Semiconductor Field-Effect Transistor
IGBT	Insulated-Gate Bipolar Transistor

Acknowledgments

The authors would like to acknowledge Department of Renewable Energy, National Advance School of Engineering of Maroua, University of Maroua.

Author Contributions

Yaouba: Conceptualization, Formal Analysis, Methodology, Resources, Software, Writing – original draft, Writing – review & editing

Albert Ayang: Conceptualization, Formal Analysis, Methodology, Resources, Software, Writing – original draft, Writing – review & editing

Ahmat Tom: Supervision, Validation

Noël Djongyang: Project administration, Supervision, Validation

Conflicts of Interest

The authors declare no conflicts of interest.

References

[1] T. Kousksou, P. Bruel, A. Jamil, T. El Rha, and Y. Zeraouli, "Solar Energy Materials & Solar Cells Energy storage : Applications and challenges," *Sol. energy Mater. Sol. cells*, vol. 120, pp. 59–80, 2014, http://dx.doi.org/10.1016/j.solmat.2013.08.015

[2] M. P. Clark *et al.*, "Characterizing Uncertainty of the Hydrologic Impacts of Climate Change," *Curr. Clim. Chang. Reports*, vol. 2, no. 2, pp. 55–64, 2016, https://doi.org/10.1007/s40641-016-0034-x

[3] A. D. Dhass, N. Beemkumar, S. Harikrishnan, and H. M. Ali, "A Review on Factors Influencing the Mismatch Losses in Solar Photovoltaic System," *Int. J. Photoenergy*, vol. 2022, 2022, https://doi.org/10.1155/2022/2986004

[4] T. F. Wu, C. H. Chang, L. C. Lin, and C. L. Kuo, "Power loss comparison of single- and two-stage grid-connected photovoltaic systems," *IEEE Trans. Energy Convers.*, vol. 26, no. 2, pp. 707–715, 2011, https://doi.org/10.1109/TEC.2011.2123897

[5] S. Daliento *et al.*, "Monitoring, diagnosis, and power forecasting for photovoltaic fields: A review," *Int. J. Photoenergy*, vol. 2017, 2017, https://doi.org/10.1155/2017/1356851

[6] A. Livera, M. Theristis, G. Makrides, and G. E. Georghiou, "Recent advances in failure diagnosis techniques based on performance data analysis for grid-connected photovoltaic systems," *Renew. Energy*, vol. 133, pp. 126–143, 2019, https://doi.org/10.1016/j.renene.2018.09.101

[7] H. Kazemi and A. Yazdizadeh, "Optimal state estimation and fault diagnosis for a class of nonlinear systems," *IEEE/CAA J. Autom. Sin.*, vol. 7, no. 2, pp. 517–526, 2020, https://doi.org/10.1109/JAS.2020.1003051

[8] J. Han, "From PID to active disturbance rejection control," *IEEE Trans. Ind. Electron.*, vol. 56, no. 3, pp. 900–906, 2009, https://doi.org/10.1109/TIE.2008.2011621

[9] D. Kharrat, H. Gassara, A. El Hajjaji, and M. Chaabane, "Adaptive Observer and Fault Tolerant Control for Takagi-Sugeno Descriptor Nonlinear Systems with Sensor and Actuator Faults," *Int. J. Control. Autom. Syst.*, vol. 16, no. 3, pp. 972–982, 2018, https://doi.org/10.1007/s12555-017-0546-8

[10] X. J. Li, J. J. Yan, and G. H. Yang, "Adaptive Fault Estimation for T-S Fuzzy Interconnected Systems Based on Persistent Excitation Condition via Reference Signals," *IEEE Trans. Cybern.*, vol. 49, no. 8, pp. 2822–2834, 2019, https://doi.org/10.1109/TCYB.2018.2820001

[11] Z. Gao, X. Shi, and S. X. Ding, "Fuzzy state/disturbance

observer design for T-S fuzzy systems with application to sensor fault estimation," *IEEE Trans. Syst. Man, Cybern. Part B Cybern.*, vol. 38, no. 3, pp. 875–880, 2008, https://doi.org/10.1109/TSMCB.2008.917185

[12] X. Liu, Z. Gao, and M. Z. Q. Chen, "Takagi-Sugeno Fuzzy Model Based Fault Estimation and Signal Compensation with Application to Wind Turbines," *IEEE Trans. Ind. Electron.*, vol. 64, no. 7, pp. 5678–5689, 2017, https://doi.org/10.1109/TIE.2017.2677327

[13] F. Benyamina, A. Benrabah, F. Khoucha, M. F. Zia, Y. Achour, and M. Benbouzid, "An augmented state observer-based sensorless control of grid-connected inverters under grid faults," *Int. J. Electr. Power Energy Syst.*, vol. 133, no. December 2020, p. 107222, 2021, https://doi.org/10.1016/j.ijepes.2021.107222

[14] M. Liu, X. Cao, and P. Shi, "Fuzzy-model-based fault-tolerant design for nonlinear stochastic systems against simultaneous sensor and actuator faults," *IEEE Trans. Fuzzy Syst.*, vol. 21, no. 5, pp. 789–799, 2013, https://doi.org/10.1109/TFUZZ.2012.2224872

[15] M. Li, M. Liu, Y. Zhang, and Y. Geng, "Fault tolerant sliding mode control for T-S fuzzy stochastic time-delay system via a novel sliding mode observer approach," *Int. J. Syst. Sci.*, vol. 49, no. 7, pp. 1353–1367, 2018, https://doi.org/10.1080/00207721.2018.1447168

[16] H. Zhang, J. Han, Y. Wang, and X. Liu, "Sensor Fault Estimation of Switched Fuzzy Systems With Unknown Input," *IEEE Trans. Fuzzy Syst.*, vol. 26, no. 3, pp. 1114–1124, 2018, https://doi.org/10.1109/TFUZZ.2017.2704543

[17] J. Lan and R. J. Patton, "Integrated Design of Fault-Tolerant Control for Nonlinear Systems Based on Fault Estimation and T-S Fuzzy Modeling," *IEEE Trans. Fuzzy Syst.*, vol. 25, no. 5, pp. 1141–1154, 2017, https://doi.org/10.1109/TFUZZ.2016.2598849

[18] Q. Jia, W. Chen, Y. Zhang, and H. Li, "Fault reconstruction and fault-tolerant control via learning observers in Takagi-Sugeno fuzzy descriptor systems with time delays," *IEEE Trans. Ind. Electron.*, vol. 62, no. 6, pp. 3885–3895, 2015, https://doi.org/10.1109/TIE.2015.2404784

[19] Q. Jia, W. Chen, Y. Zhang, and H. Li, "Fault reconstruction for Takagi-Sugeno fuzzy systems via learning observers," *Int. J. Control*, vol. 89, no. 3, pp. 564–578, 2016, https://doi.org/10.1080/00207179.2015.1086025

[20] W. H. Chen, D. J. Ballance, P. J. Gawthrop, and J. O'Reilly, "A nonlinear disturbance observer for robotic manipulators," *IEEE Trans. Ind. Electron.*, vol. 47, no. 4, pp. 932–938, 2000, https://doi.org/10.1109/41.857974

[21] S. J. Kwon and W. K. Chung, "A discrete-time design and analysis of perturbation observer for motion control applications," *IEEE Trans. Control Syst. Technol.*, vol. 11, no. 3, pp. 399–407, 2003, https://doi.org/10.1109/TCST.2003.810398

[22] J. H. She, M. Fang, Y. Ohyama, H. Hashimoto, and M. Wu, "Improving disturbance-rejection performance based on an equivalent-input-disturbance approach," *IEEE Trans. Ind. Electron.*, vol. 55, no. 1, pp. 380–389, 2008, https://doi.org/10.1109/TIE.2007.905976

[23] Z. Gao, Y. Huang, and J. Han, "An alternative paradigm for control system design," *Proc. IEEE Conf. Decis. Control*, vol. 5, pp. 4578–4585, 2001, https://doi.org/10.1109/CDC.2001.980926

[24] W. H. Chen, J. Yang, L. Guo, and S. Li, "Disturbance-Observer-Based Control and Related Methods - An Overview," *IEEE Trans. Ind. Electron.*, vol. 63, no. 2, pp. 1083–1095, 2016, https://doi.org/10.1109/TIE.2015.2478397

[25] S. Li, J. Yang, W. H. Chen, and X. Chen, "Generalized extended state observer based control for systems with mismatched uncertainties," *IEEE Trans. Ind. Electron.*, vol. 59, no. 12, pp. 4792–4802, 2012, https://doi.org/10.1109/TIE.2011.2182011

[26] P. Shah and B. Singh, "Adaptive Observer Based Control for Roof-Top Solar PV System," *IEEE Trans. Power Electron.*, vol. 35, no. 9, pp. 9402–9417, 2020, https://doi.org/10.1109/TPEL.2019.2898038.

[27] M. Alshiekh, A. Marouf, and M. Kubeitari, "Current Control and Active Damping for Single Phase LCL-Filtered Grid Connected Inverter," *J. Control Sci. Eng.*, vol. 2020, 2020, https://doi.org/10.1155/2020/3164601

[28] M. Mokhlis, M. Ferfra, and R. El Idrissi, "High gain observer-based control for grid-connected pv system under partial shading effect," *Int. J. Intell. Eng. Syst.*, vol. 13, no. 2, pp. 161–181, 2020, https://doi.org/10.22266/ijies2020.0430.16

[29] J. Wang, S. Li, J. Yang, B. Wu, and Q. Li, "Extended state observer-based sliding mode control for PWM-based DC-DC buck power converter systems with mismatched disturbances," *IET Control Theory Appl.*, vol. 9, no. 4, pp. 579–586, 2015, https://doi.org/10.1049/iet-cta.2014.0220

[30] B. Wang, Z. Shen, H. Liu, and J. Hu, "Linear ADRC direct current control of gridconnected inverter with LCL filter for both active damping and grid voltage induced current distortion suppression," *IET Power Electron.*, vol. 11, no. 11, pp. 1748–1755, 2018, https://doi.org/10.1049/iet-pel.2017.0787

[31] Y. Zhu and J. Fei, "Disturbance Observer Based Fuzzy Sliding Mode Control of PV Grid Connected Inverter," *IEEE Access*, vol. 6, pp. 21202–21211, 2018, https://doi.org/10.1109/ACCESS.2018.2825678

[32] B. Guo, S. Bacha, M. Alamir, A. Hably, and C. Boudinet, "Generalized Integrator-Extended State Observer with Applications to Grid-Connected Converters in the Presence of Disturbances," *IEEE Trans. Control Syst. Technol.*, vol. 29, no. 2, pp. 744–755, 2021, https://doi.org/10.1109/TCST.2020.2981571

[33] P. Jain *et al.*, "A luenberger observer-based fault detection and identification scheme for photovoltaic DC-DC converters," *Proc. IECON 2017 - 43rd Annu. Conf. IEEE Ind. Electron. Soc.*, vol. 2017-Janua, pp. 5015–5020, 2017, https://doi.org/10.1109/IECON.2017.8216866

[34] L. Qin, "Control of Single Phase LCL Photovoltaic Grid-Gonnected Inverter Based on State Observer," *Proc. 2020 IEEE Int. Conf. Power, Intell. Comput. Syst. ICPICS 2020*, pp. 762–765, 2020, https://doi.org/10.1109/ICPICS50287.2020.9202286

[35] A. Ayang, "Diagnostic d'un système photovoltaïque à stockage par estimation paramétrique et commandes ADRC, intégré à une centrale autonome de cogénération d'énergie," 2020. [Online]. Available: https://constellation.uqac.ca/6499/1/Ayang_uqac_0862D_10767.pdf

[36] L. Zhou, L. Cheng, C. Pan, and Z. Jiang, "Generalized Extended State Observer Based Speed Control for DC Motor Servo System," *Chinese Control Conf. CCC*, vol. 2018-July, pp. 221–226, 2018, https://doi.org/10.23919/ChiCC.2018.8483964

[37] M. A. Khan, S. Member, A. Haque, S. Member, and V. S. Bharath, "Dynamic Voltage Support for Low Voltage Ride Through Operation in Single-Phase Grid-Connected Photovoltaic Systems," *IEEE Trans. Power Electron.*, vol. 8993, no. c, 2021, https://doi.org/10.1109/TPEL.2021.3073589

[38] S. Sarikh, M. Raoufi, A. Bennouna, and B. Ikken, "Characteristic curve diagnosis based on fuzzy classification for a reliable photovoltaic fault monitoring," *Sustain. Energy Technol. Assessments*, vol. 43, no. December 2020, p. 100958, 2021, https://doi.org/10.1016/j.seta.2020.100958

[39] H. Renaudineau, J. Martin, S. Member, and S. Pierfederici, "DC-DC Converters Dynamic Modeling with State Observer-Based Parameter Estimation," *EEE Trans. POWER Electron.*, vol. 8993, no. c, pp. 1–9, 2014, https://doi.org/10.1109/TPEL.2014.2334363

[40] R. Errouissi and A. Al-durra, "Extended high-gain observer-based DC-link voltage regulation in dual-stage grid-tied PV system under balanced and unbalanced voltages," *IET Renew. Power Gener.*, vol. 14, no. 12, pp. 2037–2046, 2020, https://doi.org/10.1049/iet-rpg.2019.0973

[41] L. Xu, R. Ma, S. Zhuo, R. Xie, X. Wang, and Y. Huangfu, "Observer Based Switch Open-Circuit Diagnosis for Interleaved Boost Converter," *IECON Proc. (Industrial Electron. Conf.*, vol. 2020-Octob, pp. 5012–5017, 2020, https://doi.org/10.1109/IECON43393.2020.9254750

[42] B. Wang, Y. Xu, Z. Shen, J. Zou, C. Li, and H. Liu, "Current Control of Grid-Connected Inverter with LCL Filter Based on Extended-State Observer Estimations Using Single Sensor and Achieving Improved Robust Observation Dynamics," *IEEE Trans. Ind. Electron.*, vol. 64, no. 7, pp. 5428–5439, 2017, https://doi.org/10.1109/TIE.2017.2674600

[43] W. Xue, W. Bai, S. Yang, and K. Song, "ADRC With Adaptive Extended State Observer and its Application to Air – Fuel Ratio Control in Gasoline Engines," *IEEE Trans. Ind. Electron.*, vol. 62, no. August, pp. 5847–5857, 2015, https://doi.org/10.1109/TIE.2015.2435004

[44] Yaouba *et al.*, "An Experimental and Case Study on the Evaluation of the Partial Shading Impact on PV Module Performance Operating Under the Sudano-Sahelian Climate of Cameroon," *Front. Energy Res.*, vol. 10, no. August, pp. 1–13, 2022, https://doi.org/10.3389/fenrg.2022.924285

[45] L. Zhou, L. Cheng, J. She, and Z. Zhang, "Generalized extended state observer–based repetitive control for systems with mismatched disturbances," *Int. J. Robust Nonlinear Control*, vol. 29, no. 11, pp. 3777–3792, 2019, https://doi.org/10.1002/rnc.4582

[46] R. Madoński and P. Herman, "Survey on methods of increasing the efficiency of extended state disturbance observers," *ISA Trans.*, vol. 56, pp. 18–27, 2015, https://doi.org/10.1016/j.isatra.2014.11.008

[47] M. A. Mahmud, H. R. Pota, M. J. Hossain, and S. Member, "Nonlinear Current Control Scheme for a Single-Phase Grid-Connected Photovoltaic System," *IEEE Trans. Sustain. ENERGY*, vol. 5, no. 1, pp. 218–227, 2014, https://doi.org/10.1109/TSTE.2013.2279884